Nano Research

Open Access

Review Article

Synthesis, morphological control and catalytic application of nanomaterials containing poly(ionic liquid)s

Shunyu Yao[1], Songming Yang[2]✉, and Jinying Yuan[2]✉

[1] *Zhili College, Tsinghua University, Beijing 100084, China*
[2] *Key Lab of Organic Optoelectronics and Molecular Engineering of Ministry of Education Department of Chemistry, Tsinghua University, Beijing 100084, China*

Cite this article: *Nano Research*, **2026**, *19*, 94908511. https://doi.org/10.26599/NR.2026.94908511

ABSTRACT: Nano materials based on poly(ionic liquid)s (PILs) have been extensively studied in recent decades due to their unique abilities in morphological control and applications in catalysts. The self-assembly of PILs enables the formation of diverse nanostructures (such as spheres or vesicles), typically exhibiting high specific surface areas, which are highly desirable in catalysis. This review first summarizes common synthetic methods for PILs and then focuses on explaining the principles of PIL self-assembly and strategies for morphology control, while also comparing different self-assembly approaches. Furthermore, from a macroscopic perspective, applications of PILs in catalysis are discussed, coupled with particular emphasis on comparing their roles in composite materials, highlighting their irreplaceable function in heterogeneous catalytic systems. Finally, current research challenges and perspectives on future developments of PILs are also presented.

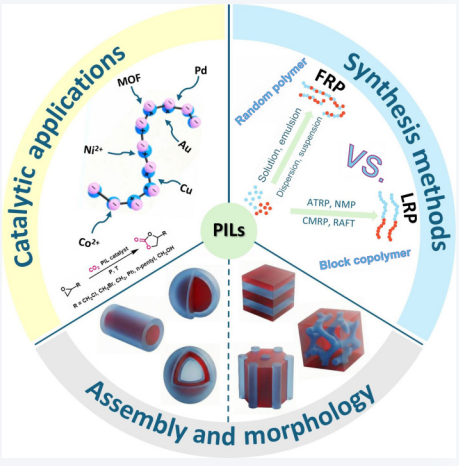

KEYWORDS: poly(ionic liquid), self-assembly, morphological control, catalyst

1 Introduction

Ionic liquids (ILs), defined as organic salts that are entirely composed of cations and anions and remain in a liquid state at or near room temperature (typically below 100 °C), have rapidly emerged as promising materials due to their unique physicochemical properties, such as high thermal and chemical stability due to their unique strong charge interactions, negligible vapor pressure, and high ionic conductivity. Poly(ionic liquid)s (PILs), on the other hand, are polyelectrolytes consisting of polymer backbones with repeating units of IL monomers. Many of the characteristic advantages of ILs are retained in PILs after polymerization. Moreover, the structural designability of IL monomers enables functionalization of PILs, making them an attractive subject in the field of materials chemistry [1–3].

Early studies on PILs have explored various aspects such as synthesis strategies, molecular design, and material applications. For instance, in 2011, Mecerreyes investigated the synthesis of PILs along with their properties in both solution and solid states [4]. In 2017, Yan's research group provided a comprehensive review on the synthesis, assembly methods, and applications of PILs in materials and biological sciences [5].

However, despite the rapid development of PIL research in recent years, there remains a lack of systematic reviews focusing on the synthesis, morphology control, and functional applications of PIL-based nanomaterials. Therefore, this review summarizes recent advances in the preparation of PIL-based nanomaterials, the regulation of their microstructures, and their applications in catalysis. Emphasis is placed on important recent work in the following areas: (1) representative synthesis methods; (2) morphological control and assembly methods; and (3) the advantages of PIL nanoparticles in catalytic reactions.

2 Synthesis of PILs

Different structures of PILs guarantee their diverse applications of PILs across various fields. Generally, the standard synthetic routes for PILs are based on the following fundamental strategies: (1) IL monomers directly polymerized via chain-growth polymerization

Received: December 7, 2025; **Revised:** January 29, 2026
Accepted: January 30, 2026

✉Address correspondence to Songming Yang, yangsm24@mails.tsinghua.edu.cn; Jinying Yuan, yuanjy@mail.tsinghua.edu.cn

methods like free radical polymerization (FRP) or cationic polymerization, etc. It is also important to note that the properties of IL monomers can be tailored through pre-modification or functionalization, thereby enabling their use in a wider range of applications. (2) Conventional polymers can be modified to synthesize PILs through methods such as addition reactions [5, 6].

The evolution of polymerization methodologies over recent decades has significantly expanded beyond FRP. The current toolkit now includes specialized techniques like cationic polymerization [7], as well as advanced methods such as microwave-assisted polymerization [8]. In this section, widely used synthetic strategies including FRP and living radical polymerization (LRP) will be listed and briefly introduced.

FRP is known for its simplicity, high reaction rate and relatively mild reaction conditions. It offers exceptionally broad adaptability, as it is compatible with a wide range of monomers, has a high tolerance towards impurities, and is cost-effective [9]. These advantages also imply enhanced editability and functionalization of the resulting polymers. As a result, FRP remains one of the most widely used synthetic approaches, both in laboratory research and industrial production. Common FRP methods include solution polymerization [10–12], emulsion polymerization [13], suspension polymerization [14] and dispersion polymerization [15].

However, FRP is very difficult to modulate due to the explosive nature of the chain-growth process, which results in uncontrollable chain lengths, degree of polymerization and high polymer dispersity index (PDI). On the other hand, LRP, as a novel approach to radical polymerization, has significantly mitigated the drawbacks associated with conventional FRP. By establishing a reversible deactivation/activation equilibrium, LRP effectively suppresses bimolecular termination. Consequently, the molecular weight of the resulting polymers exhibits a linear relationship with monomer conversion, and the molecular weight distribution is narrow. The minimal presence of "dead chains" also enables further chain extension or block copolymerization. This high degree of designability and controllability makes LRP particularly suitable for the precise synthesis of advanced polymeric materials. Moreover, the ability of LRP to fabricate block copolymers is also highly appreciated. Commonly used LRP methods include nitroxide-mediated radical polymerization (NMP) [16, 17], cobalt meditated living polymerization (CMRP) [18], atom transfer radical polymerization (ATRP) [19, 20], reversible addition-fragmentation chain transfer polymerization (RAFT) [21, 22].

3 Controlled morphologies of PILs

Self-assembly stands as one of the most powerful strategies for constructing complex and ordered nanomaterials. Polymers serve as the primary materials enabling self-assembly, and they play critical roles in various modern technologies such as drug delivery [23], smart coatings [24], and nano reactors [25]. Among these, PILs have attracted significant attention due to their unique physicochemical properties. Research on PILs has not only focused on applications like solid electrolytes [26], adsorbents [27], and gel-based sensors [28], but also pays attention to their self-assembly behaviors.

This section explores the self-assembly of PILs by analyzing the factors that will influence the ultimate morphologies of the assemblies and list several common assembly methods.

3.1 Classification of different morphologies

Spheres: The self-assembly of ionic liquids can yield diverse morphologies. Conventionally, solid spheres are considered elementary morphologies. This is because first, the solvophobic segments aggregate to form a core shielded from the solvent by the solvophilic segments. To minimize energy, this core adopts a spherical shape, as a sphere has the smallest surface area for a given volume. Second, kinetically, spheres have the lowest energy barrier for formation and assemble the fastest. This can be proved by some dynamic simulation methods, like external potential dynamics (EPD) methods [29].

More advanced nano assemblies: Other more complex morphologies include worms, rods, and vesicles, etc., which hold significant advantages in catalysis and substance transport or loading due to their internal cavities and unique membrane structures. The above morphologies are usually deemed as advanced because of their more potential applications.

While the aforementioned morphologies characterize individual nano-assemblies, their organization via external stimuli (e.g., solvent evaporation) can yield an emergent class of macroscopic solids with unique superstructures. Compared to the primary assemblies, these hierarchical architectures present superior processability and possess monolithic, continuous physicochemical characteristics. Examples include lamellae, hexagonal columnar, three-dimensional networks, etc. For PIL-based assemblies, additional features such as ion transport capability and electrical conductivity distinguish them from conventional membranes or gels. These properties are also superior to those of isolated micelles. For instance, in lamellae structures, ions can undergo rapid directional transport along hydrophilic layers; in bi-continuous phases, both electrons and ions can migrate efficiently through their respective channels, significantly enhancing overall performance.

Lamellae: The bilayer membrane is considered the fundamental building block of the lamellae phase. The driving force behind the film formation process is like that of PIL self-assembly: Microphase separation serves as the core mechanism, during which electrostatic interactions and π–π stacking promote highly ordered lamellar packing. The key to form a lamellae structure lies in the necessity of solvent evaporation. Throughout this process, the concentration of PILs increases drastically, amplifying intermolecular interactions and forcing molecular rearrangement, thereby leading to an ordered and stable membrane structure.

Hexagonal cylinder: Like lamellae morphology, hexagonal cylindrical morphology is also a self-assembled system with a symmetrical structure. This type of self-assembly is commonly observed in BCPs when the volume fractions of the two components are unequal, with the minority component forming the cylindrical domains. It consists of cylindrical/columnar microdomains regularly (or approximately regularly) embedded within a continuous matrix of the other component, where the cylinders are arranged in a hexagonal closely packed pattern. Here, the matrix refers to the continuous-phase polymer block, not a solvent. Due to the uniformity of the assembly, its structure is continuous and symmetrical. A key result of this structure is its high anisotropy: Many properties differ significantly along the axis of the cylinders compared to directions perpendicular to it. In the presence of PILs, unidirectional conductivity becomes even more pronounced.

Three-dimensional network: Here, the term "three-dimensional network" specifically refers to a three-dimensional bi-continuous

phase. In terms of continuity, both lamellae and hexagonally packed cylindrical morphologies are continuous in only one dimension, resulting in anisotropic physicochemical properties. In contrast, the three-dimensional network is isotropic, meaning it exhibits superior mechanical properties and conductivity. This makes such a structure highly promising for applications as solid-state electrolytes. Apart from conductivity, three-dimensional networks, which typically exhibit negative Gaussian curvature, offer the dual advantages of intrinsic mechanical stability and a high specific surface area. This synergistic effect makes them exceptionally advantageous for adsorption and separation applications.

Two most common types of three-dimensional network structures are the gyroid structure (space group *Ia3d*) and the double diamond structure (space group *Pn3m*). The primary difference between them is that the former consists of two identical yet non-intersecting chiral networks. These two networks are chiral enantiomers of each other and can be visualized as a network formed by trident-shaped connection points. In contrast, the latter is composed of two interpenetrating three-dimensional networks that are identical, with connection points resembling the bonding arrangement of carbon atoms in diamond. In terms of applications, the gyroid structure holds more advantages in areas such as ion transport, adsorption, and chiral separation. This is attributed to its intrinsically chiral network, generally higher specific surface area, and lower tortuosity. In contrast, the double diamond phase possesses a wider complete photonic bandgap due to its unique symmetry, granting it potential applications in photonic crystals. In practice, the gyroid structure is more readily attainable than the double diamond phase, as the latter has a very narrow formation window. This point will be mentioned in the bulk assembly section (Section 3.3.2.1).

From a synthetic perspective, obtaining PILs with the potential to self-assemble into these morphologies requires the use of different methods. For instance, FRP is employed when subsequent polymerization requirements are less demanding, whereas the precise synthesis of BCPs necessitates LRP. More detailed studies are summarized in Table 1.

3.2 Driving forces and molecular design

The self-assembly of PILs is a process synergistically driven by multiple intermolecular interactions, and their designability at the molecular level enables precise regulation of these interactions, thereby facilitating control over the final nanostructures.

Microphase separation is defined as a spontaneous and confined phase separation that occurs in block copolymers (BCPs) or molecules with analogous structures, due to the thermodynamic incompatibility between their different blocks, leading to the formation of regular nanostructures. Some calculation simulations have been put forward like self-consistent field theory [43]. Self-assembly serves as a manifestation of microphase separation but is not limited to BCPs. There are four primary driving forces for self-assembly: electrostatic interactions, hydrophobic interactions, π–π stacking interactions, and hydrogen bonding. According to the aforementioned driving forces, some methods to adjust the self-assembly of PILs can be put forward. The most employed strategies involve modulating the alkyl chain length of the IL monomer side chains and adjusting the counterions.

3.2.1 Changing side chain structure

An early work published by Antonietti's research group in 2011 demonstrated the flexibility of altering alkyl chain length. In this work, vinylimidazolium-based PILs with alkyl chain lengths varying from C12 to C18 were synthesized. The morphological evolution progresses from concentric multilamellar assemblies (C12/C14) to faceted unilamellar structures (C16/C18) with extended alkyl chains. Figure 1 shows cryo-TEM figures of PILs assemblies with different alkyl chain length. Influence of assembly concentration is obvious. At a concentration of 100 g·L^{-1}, the C12 derivative spontaneously self-assembles into nanoworm-like superstructures [44].

The work of Antonietti's group marked a pioneering milestone of self-assembly of single-component PILs. A lot more work has emerged after this, and various kinds of systems were exploited. For example, Yuan's group extended their research field into triazole-based PILs in 2016. 1-Vinyl-1,2,4-triazolium-based PILs were synthesized, including 4-n-dodecyl-1-vinyl-1,2,4-triazolium iodide (TILM-C12I), 4-n-dodecyl-1-vinyl-1,2,4-triazolium bromide (TILM-C12Br) and its longer alkyl chain derivatives. A morphological evolution from "wasp-like" striped ellipsoids to "onion-like" multilamellar vesicles was observed (Fig. 2). The different behaviors in assembly are probably because of the higher polarity of triazole than that of imidazolium. The assemblies in this work exhibit pronounced pH-responsive behavior. Under alkaline conditions (high pH), nanoparticle aggregation occurs due to reduced ζ-potential, while acidic conditions (low pH) trigger redispersion. This demonstrates pH-tunable colloidal stability [45].

The next year, Vijayakrishna's group synthesized poly(N-imidazole-3-propylmethacrylamide) (P(ImPMAm)) through RAFT polymerization in water. Morphologies of the self-assembled polymers with alkyl and phenethyl side chains exhibited distinct structural features, forming unilamellar vesicles and onion-like multilamellar vesicles, respectively (Fig. 3). These assemblies can be applied as both catalyst carriers and coating encapsulation matrices. In this work, the elimination of RAFT end groups greatly affected the morphologies of the assemblies. Rod-like (end groups eliminated) and vesicle (end groups reserved) structures were observed. For catalytic usage, Ag nanoparticles are basically affiliated with hydrophilic chains [46].

To vary the sorts of solvents in the assembly system, the latest research of Mandal's group in 2025 reported the synthesis of quaternary ammonium PILs with long alkyl chain functionalities, which self-assembled into vesicles with a broad size distribution in chloroform. A vital application of these assemblies is capsulation of certain hydrophilic dyes (Eosin B). Due to its solvophobic nature, Eosin B dye exhibits favorable compatibility with the solvophobic cores of vesicles. This unique polarity matching enables efficient dye encapsulation within these vesicles. The length of alkyl chains mainly influences the size of the vesicles assembled but didn't change the morphology [47].

Based on the studies discussed above, the alkyl chain exerts a significant influence on the self-assembly of single-component PILs. Regardless of whether the backbone cationic moiety is imidazolium-type, triazolium-type, or quaternary ammonium-type, as the alkyl chain length increases, the hydrophobicity enhances, which leads to the significant morphological changes. However, to the best of our knowledge, most studies on single-component PIL self-assembly do not involve the systematic use of branched alkyl chains or multiple alkyl chains. Theoretically, the steric hindrance distinct from that of linear alkyl chains may lead to different self-assembly behaviors.

3.2.2 Changing main chain structure: the construction of BCPs

It can't be denied that single-component PILs have their advantages of having relatively simple structures and having direct and quick

Table 1 A list of different synthesis methods, product structures and assembly morphologies

Synthesis method	Product structure	Assembly morphology	Reference
Solution polymerization	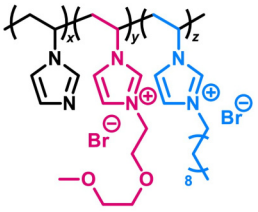	Sphere (about 100 nm)	[30]
	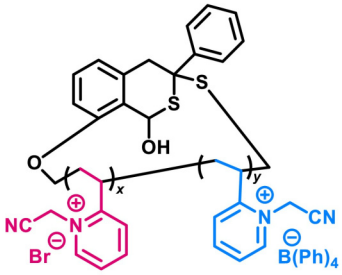	Sphere (40–250 nm)	[31]
	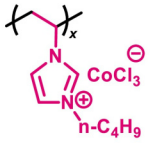	nanowire (20 nm in width)	[32]
Emulsion polymerization	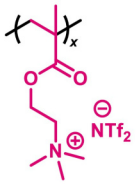	Snowman-like (about 1 μm)	[33]
Suspension polymerization	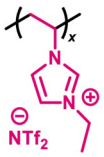	Sphere (about 5 μm)	[14]
Dispersion polymerization	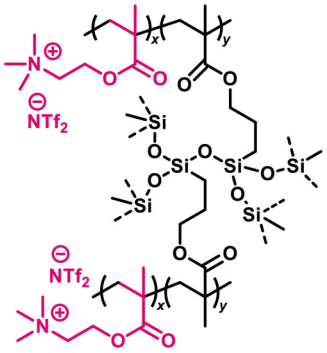	Sphere with rough shell (180 nm PIL shell, 2.4 μm NP)	[15]
ATRP	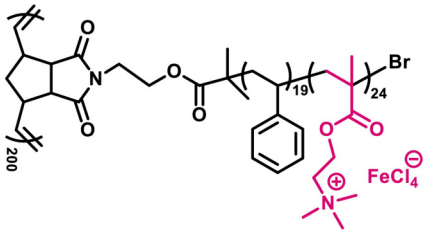	Rod (diameter: 3.3 nm length: 26.4 nm)	[19]

(Continued)

Synthesis method	Product structure	Assembly morphology	Reference
	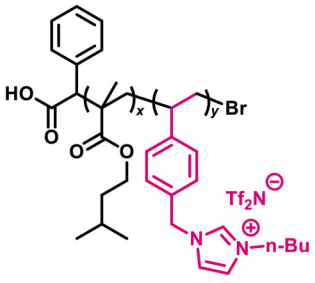	Sphere (930 nm)	[20]
	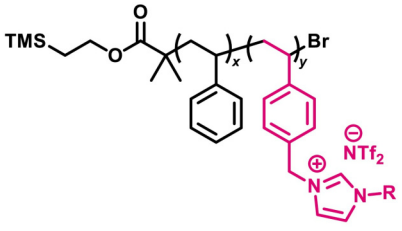	Hexagonally packed cylinders/lamellae/gyroid	[34]
CMRP	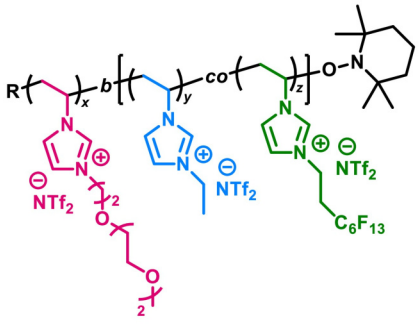	Sphere (20–60 nm)	[18]
	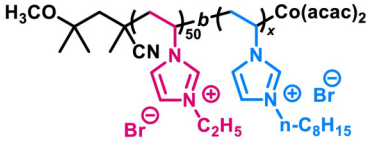	Sphere (25–80 nm)	[35]
RAFT	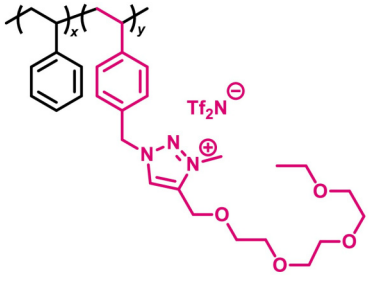	Cylinder (domain space: 31.6 nm)	[36]
	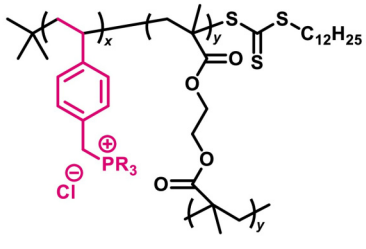	Nano ring/wire	[37]

(Continued)

Synthesis method	Product structure	Assembly morphology	Reference
Ion exchange	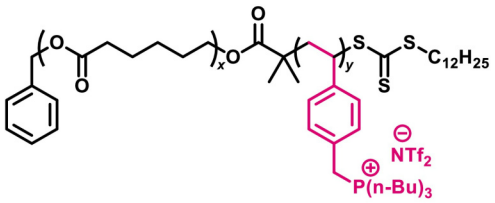	Sphere (30–60 nm)	[38]
	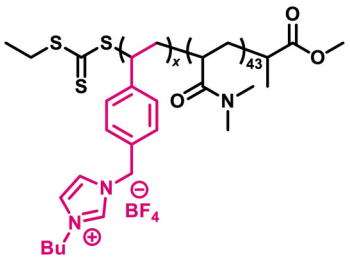	Sphere/worm/vesicle	[39]
	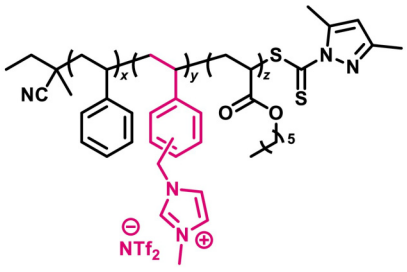	Lamellae/gyroid	[40]
	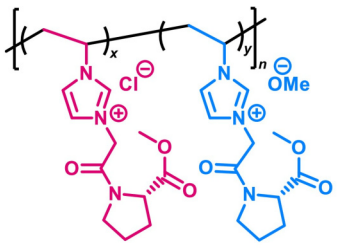	Double helix	[41]
	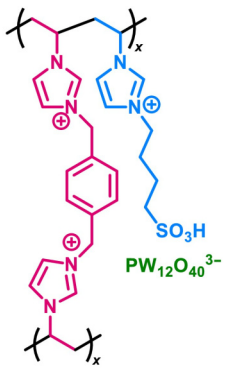	Interconnected porous structure	[42]

response to environmental changes. However, we can't neglect their problem like limited functionality, from a molecular perspective. Therefore, block copolymers are designed to grant the assemblies more functions. Not only the structures of polymers can be shifted easily (alkyl chains still affact assembly morphologies), but the morphologies can be modulated by adjusting variables such as the degree of polymerization (DP) and solid content.

Apart from BCP melts, there is also plenty of research of BCPPILs in solutions. Polymerization-induced microphase separation (PIMS) via crosslinking is a common method to obtain bi-continuous structures. However, as far as we know, most studies about PIMS applied to BCPs focus on common polymer BCPs, with the addition of ILs to the formed network to improve conductivity, instead of the direct usage of PILs [48–50]. Common

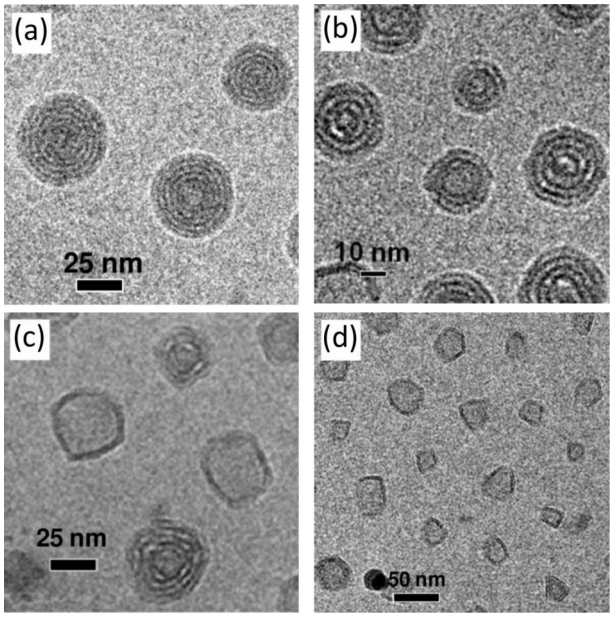

Figure 1 Representative cryo-TEM images of PIL nanoparticles in aqueous solution: (a) poly(ILM-C12), (b) poly(ILM-C14), (c) poly(ILM-C16), and (d) poly(ILM-C18). Reproduced with permission from Ref. [44], © American Chemical Society 2011.

studies involving PILs are accomplished via LRP, they enable precise control over a wide range of solid content. This leads to a scenario where, to achieve the most stable packing state within confined space, the system tends to form morphologies with higher spatial packing efficiency, thereby resulting in the formation of linear morphologies such as worm-like structures. For instance, in 2018, An's group synthesized poly(N,N-dimethylacrylamide)-*b*-1-poly(butyl-3-(4-vinylbenzyl)imidazolium tetrafluoroborate) (PDMA-*b*-P([BVBlm][BF4])) via RAFT polymerization. DPs were altered under different solid contents. A gradual change in morphology was achieved (sphere-worm-vesicle). In this process, lamellae morphology was also observed. This is because as DP increases, structures with lower curvature are more prone to form. Researchers utilized morphology diagrams to demonstrate that as both the solid content increases and the PILs block extends, the morphology of the assemblies tends to evolve toward greater complexity (Fig. 4) [39].

This work focused more on progressive morphological changes. A work in 2017 by Zhu's group used similar methods to control the self-assembly of PILs, but they paid more attention to worm-like assemblies. In their work, PEG-*b*-P(C12VIm-Br) was prepared, in which PEG-xanthate acted as a macro-CTA for RAFT/MADIX polymerization. Self-assembly of the PILs under ultra-low DPs was achieved (Fig. 5). Difference in charges of two blocks resulted in relatively easier formation of the aggregates [51].

From the two studies discussed above, we can observe that solid content and DPs serve as distinctive parameters for morphology control in BCPPILs, setting them apart from conventional single-component PILs. This distinction arises because the self-assembly of single-component PILs is predominantly a thermodynamically driven process, governed mainly by electrostatic and hydrophobic interactions. Because of this, it remains largely insensitive to variations in solid content, and the FRP synthesis method further limits precise control over the degree of polymerization. In contrast, the behavior of BCP PILs is kinetically dominated, making them

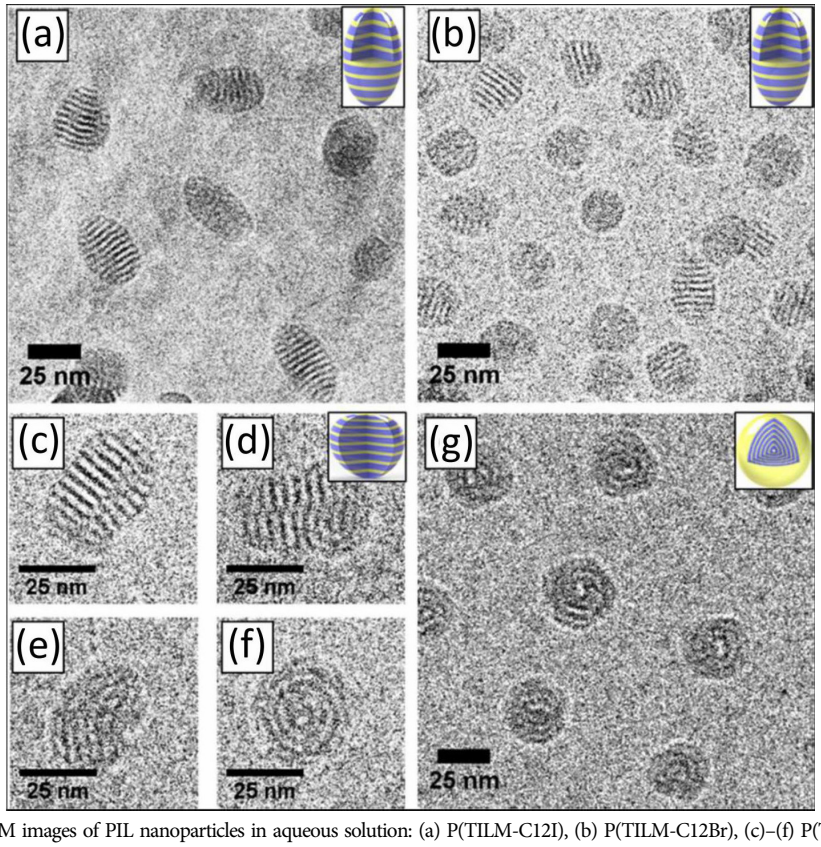

Figure 2 Representative cryo-EM images of PIL nanoparticles in aqueous solution: (a) P(TILM-C12I), (b) P(TILM-C12Br), (c)–(f) P(TILM-C14Br), and (g) P(TILM-C16Br). Reproduced with permission from Ref. [45], © American Chemical Society 2016.

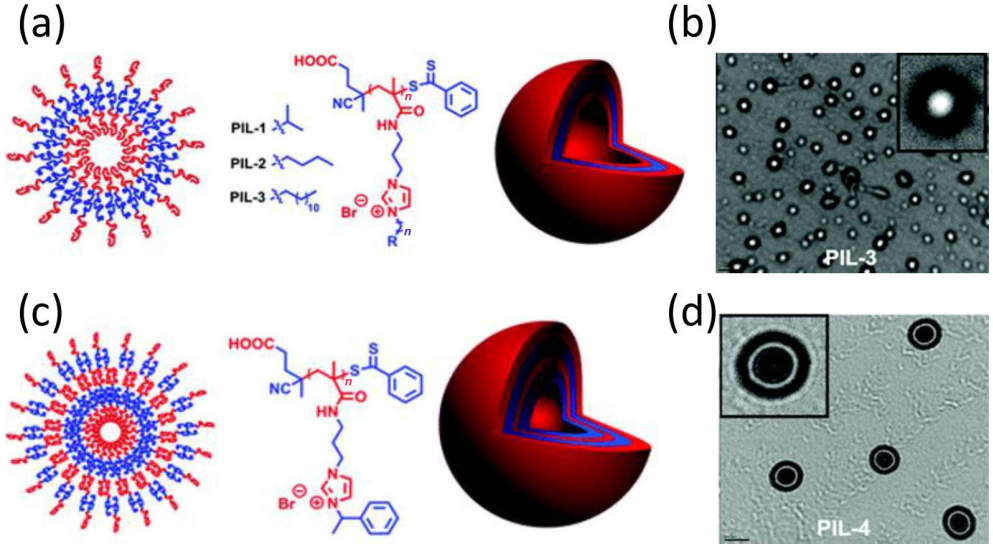

Figure 3 (a) and (c) Graphical representation of the self-assembly of PILs (1, 2, 3) and PIL-4 into vesicles in aqueous solution. (b) and (d) TEM images of the self-assembly of PIL-3 and PIL-4. Reproduced with permission from Ref. [46], © Royal Society of Chemistry 2017.

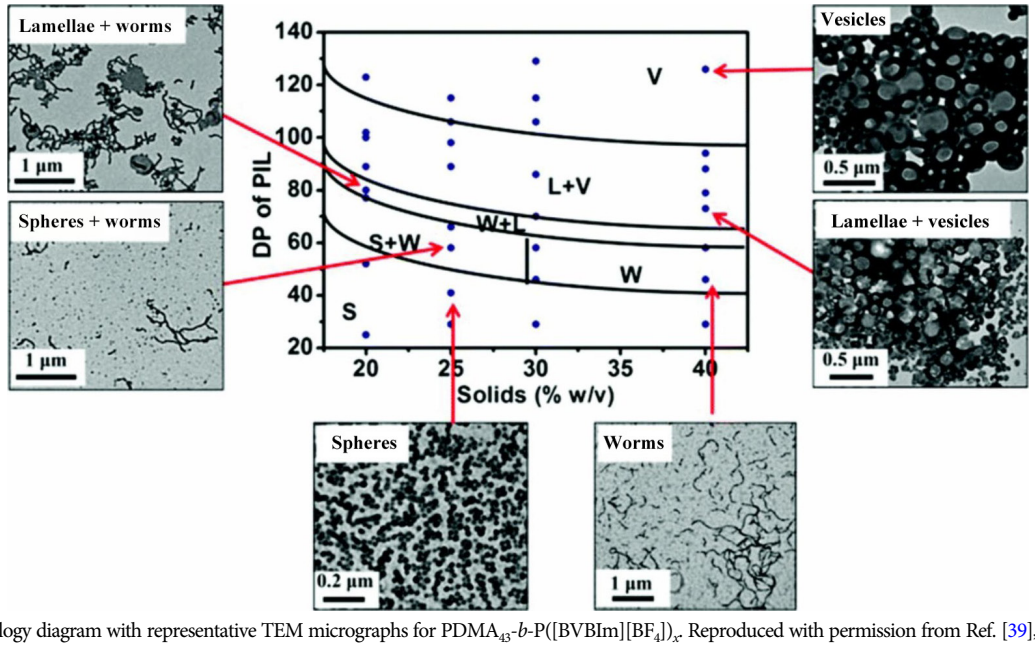

Figure 4 Morphology diagram with representative TEM micrographs for $PDMA_{43}$-*b*-P([BVBIm][BF_4])$_x$. Reproduced with permission from Ref. [39], © Royal Society of Chemistry 2018.

more responsive to solid content. Higher solid contents accelerate the kinetics of chain aggregation and rearrangement, thereby facilitating the system's transition toward more complex morphologies.

3.2.3 *Exchanging counterions*

Ion exchange is a method applied to pre-formed polymer chains, which induces morphological transformation by replacing some or all of a specific type of ion in the polymer. This approach drives self-assembly by altering the polymer's charge properties, steric hindrance, or intermolecular interactions.

In the work of Nandan's group in 2022, by functionalizing the achiral poly(4-vinylpyridine)-*b*-polystyrene (PS-*b*-P4VP) block copolymer and introducing chiral amino acids (L-/D-histidine), ionic liquid-based chiral BCPs with helical nanofibril structures were constructed. Their self-assembly behavior in both solution and bulk phases, as well as the phenomenon of helical handedness inversion, were investigated. The successful transfer of chirality from the molecular level to macroscopic helical morphologies was achieved, and a reversal of helical handedness was observed at both hierarchical levels (solution and bulk). The self-assembly process was achieved by altering the polarity of the solvent (slowly adding nonsolvent to solvent) [52].

In a recent study of Vijayakrishna's group in 2025, the single-handed helical conformation of the chiral polyelectrolyte poly-(L)-Pro-Cl was induced and amplified by partially exchanging its Cl^- ions with OMe^- ions (Fig. 6(a)). A helical conformation could be triggered with only 1 mol.% of OMe^- anion exchange. As the OMe^- content increased, a morphological evolution from featureless structures to worm-like and even double-helix-like morphologies (Figs. 6(b)–6(d)) was observed [41].

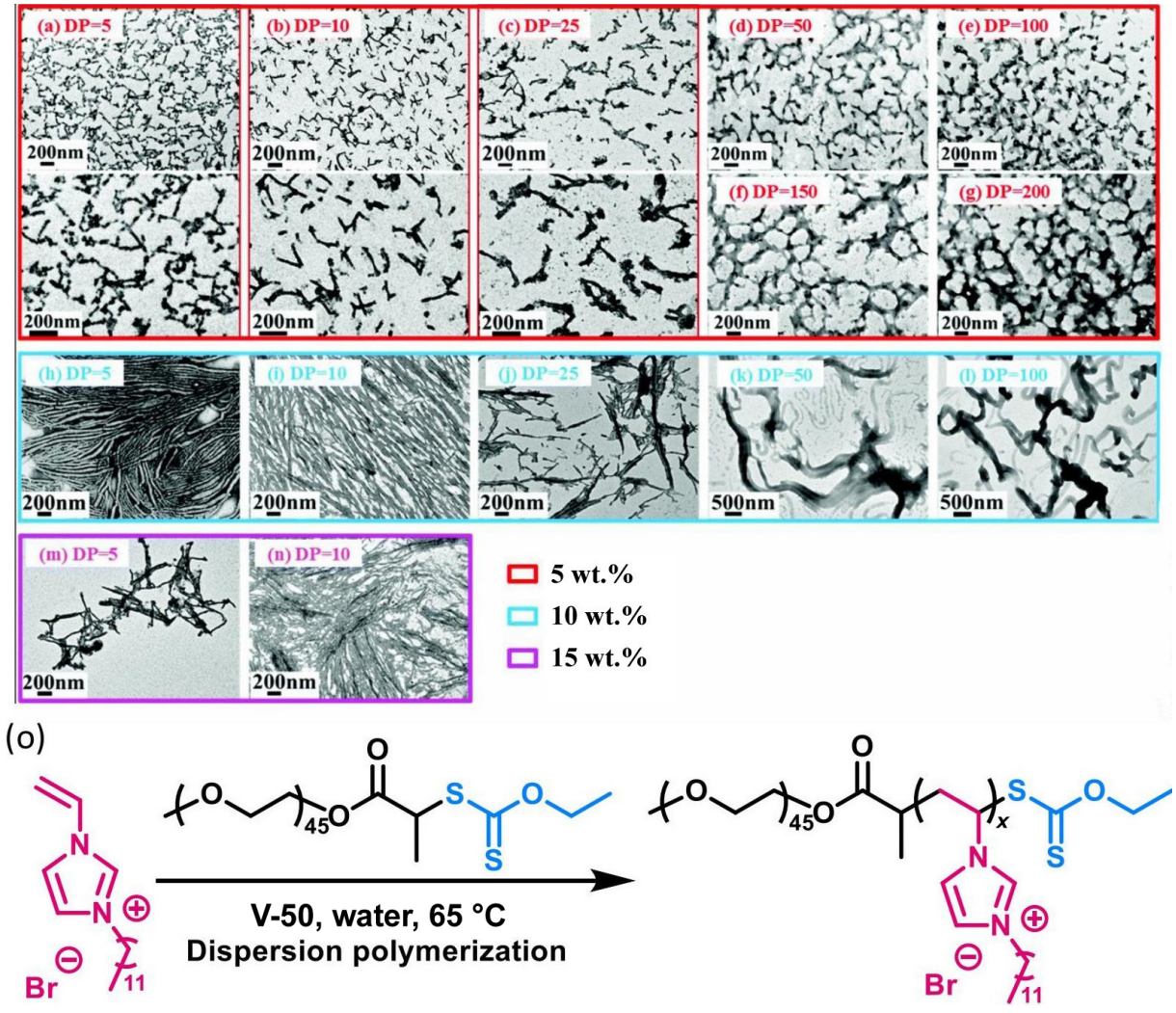

Figure 5 TEM micrographs for PEG-*b*-P(C_{12}VIm-Br)$_n$ of different DPs at solids contents of (a)–(g) 5 wt.%, (h)–(l) 10 wt.%, and ((m) and (n)) 15 wt.%. (o) Preparation of poly(ionic liquid) nanoparticles through RAFT/MADIX polymerization-induced self-assembly in water. Reproduced with permission from Ref. [51], © Royal Society of Chemistry 2017.

3.3 Assembly methods

Methods for inducing polymer self-assembly can be categorized into two types: solvent participating and bulk. The former requires a solvent medium, as exemplified by conventional post-polymerization self-assembly, polymerization-induced self-assembly (PISA), and ion-exchange processes. The latter, in contrast, proceeds without solvent involvement and can be achieved either through solvent evaporation or directly in the melt state.

3.3.1 Solvent participating

3.3.1.1 Traditional post assembly

Traditional post-assembly is a strategy that involves first synthesizing the target polymer and then triggering assembly by altering the solvent environment. The key lies in introducing a poor solvent for the PIL or a specific block to enhance hydrophobic interactions and possible electrostatic effects, thereby providing the driving force for assembly. Solvents demonstrate special selectivity towards the ultimate morphologies of the assemblies. This can be proved by the work of Nulwala's, Möller's and Matyjaszewski's group in 2017. They first reported that PILBCPs self-assembled into cuboidal nanoparticles (Fig. 7(b)) with an internal bi-continuous cubic structure in a water/THF mixed solvent system (where water is later added to the system as a poor solvent). The BCP prepared had a PAA-*b*-PIL structure (Fig. 7(a)). Within a narrow parameter window, the self-assembled morphology could be controlled by factors such as polymer concentration, solvent composition, and temperature, enabling clear observation of transitions between micelles, lamellae, multilamellar vesicles, and cubosomes. The internal structure of the cubosomes was confirmed by SAXS to be a double diamond bi-continuous phase (Figs. 7(c) and 7(d)) [53].

In the latest work of Ren's research group, they synthesized PS-*b*-QPDMA[$FeCl_4$] (Fig. 8(a)) (which was first dissolved in DMF) and investigated its self-assembly behavior in shell-selective solvent (water) and core-selective solvent (THF), respectively (Figs. 8(b)–8(d)). In the two systems, nanorods with a PS core and magnetic PIL shell, and nanospheres with a magnetic PIL core and PS shell were formed, respectively [54].

In fact, the post assembly process does not necessarily start with a solution, undergoing a change from soluble to assembling. Solid state PIL can be directly dispersed into a selective solvent. After a

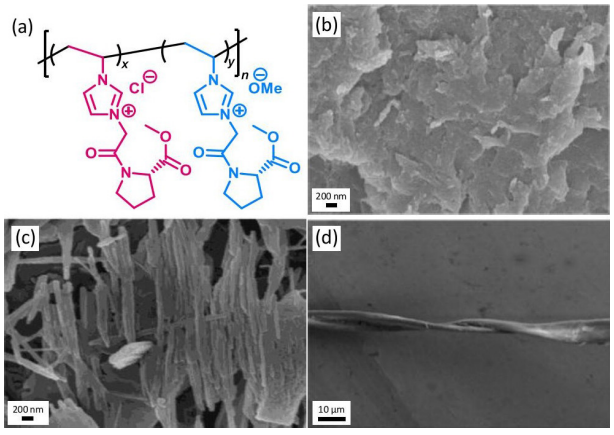

Figure 6 (a) Molecular structure of the copolymer. FESEM images at homo and random copolymers: (b) poly-(L-)-Pro-Cl, (c) poly-(L-)-Pro-$Cl_{0.9}$-*co*-poly-(L-)-Pro-$OMe_{0.1}$, and (d) poly-(L-)-Pro-OMe. Reproduced with permission from Ref. [41], © Wiley-VCH GmbH 2024.

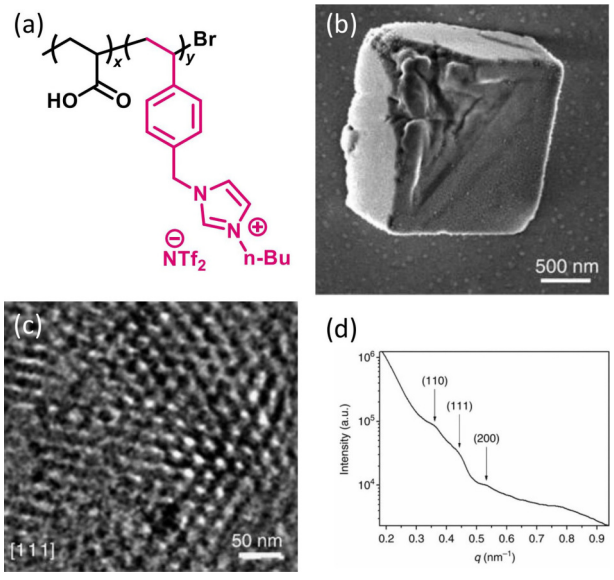

Figure 7 (a) Structure of PAA-*b*-PIL. (b) SEM micrograph of the dried cubosomes after dialysis. (c) Enlarged surface image recorded in the central area of a cuboid particle from the [111] facet. (d) SAXS diagram indicates a double diamond (*Pn3m*) lattice with a = 23.5 nm ($q/q^* \sim \sqrt{2} : \sqrt{3} : 2$). Reproduced with permission from Ref. [53], © Springer 2017.

slow and lasting stir, a relatively low concentration solution will form. However, to the best of our knowledge, although there are a few works on traditional BCPs, works applying this method to PILs are very rare. This is probably because this process demands highly of the solvent, requiring it to form assemblies in the exact domain.

3.3.1.2 Polymerization induced self-assembly

Polymerization-induced self-assembly (PISA) integrates the polymerization reaction and the self-assembly process into one single step, thereby addressing the limitations of traditional self-assembly methods, such as multiple steps, long duration, and low solid contents. Another advantage of PISA is its convenience to obtain controllable advanced morphologies. The fundamental process is as follows, using RAFT-PISA as an example. Initially, a soluble macromolecular chain transfer agent and monomer are dissolved in a selective solvent (e.g., water) or form uniform emulsions. After the initiator is introduced, the monomer

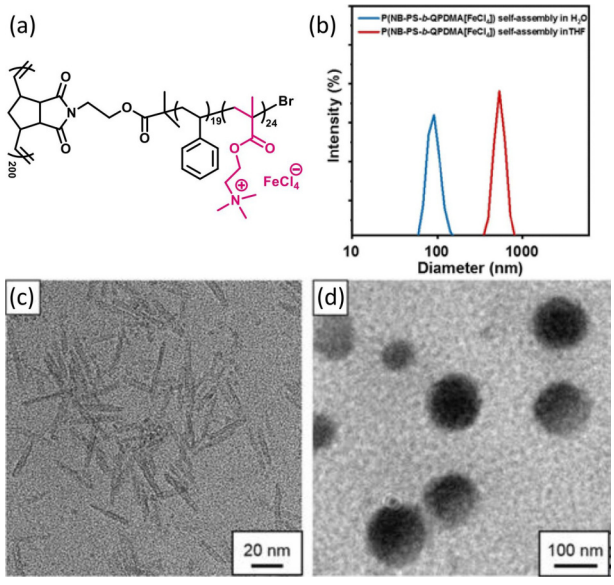

Figure 8 (a) Molecular structure of P(NB-PS-*b*-QPDMA[$FeCl_4$]). (b) Dynamic particle size of P(NB-PS-*b*-QPDMA[$FeCl_4$]) self-assembly in different solutions. HRTEM image of P(NB-PS-*b*-QPDMA[$FeCl_4$]) after self-assembly in (c) DI water and (d) THF. Reproduced with permission from Ref. [54], © Royal Society of Chemistry 2025.

polymerizes continuously, attaching to the soluble macromolecular chains to form amphiphilic block copolymers. When the length of the insoluble block reaches a certain threshold, it becomes unstable in the solvent and begins to aggregate, forming tiny cores. Meanwhile, the soluble blocks extend into the solvent, forming a protective shell. As the degree of polymerization increases, the assembled morphology evolves gradually. The abilities to achieve high solid content (up to 50%) and precisely control morphology are significant advantages of PISA.

The PISA methodology is typically combined with various synthetic approaches from LRP. Its combination with RAFT polymerization is the most prevalent. For example, in 2020, Mecerreyes's research group realized the controlled polymerization of diallyldimethylammonium chloride (DADMAC) monomer using Macromolecular Design by Interchange of Xanthate (MADIX) and RAFT techniques based on xanthate agents. In the presence of PDADMAC macromolecular CTA, the hydrophobic monomer styrene was directly polymerized in the aqueous phase, forming core–shell structured nanoparticles (NPs). By adjusting the block ratio and length, the size (diameters of 150–320 nm according to TEM results) and morphology (predominantly spherical) of the NPs were controlled. PDADMAC-*b*-PS underwent anion exchange with LiTFSI in solution to form PDADMATFSI-*b*-PS, which enhanced hydrophobicity. PDADMATFSI-*b*-PS not only surpasses conventional materials in terms of synthesis, but also significantly enhances the ionic liquid electrolyte (ILE) loading capacity, mechanical strength, and ionic conductivity at room temperature [55].

The next year, Bernard's group synthesized an all-poly(ionic liquid) (all-PIL) BCP using a pair of water-soluble isomeric imidazolium-based ionic liquid monomers 1-[2-acryloylethyl]-3-dodecylimidazolium bromide (AEDIBr) and 1-[2-acryloyldodecyl]-3-ethylimidazolium bromide (ADEIBr) as starting materials. $PAEDIBr_9$-*b*-$PADEIBr_n$ was finally prepared. The distinct water solubility behaviors of their respective polymers drove self-assembly

into diverse morphologies. A progressive evolution of morphologies—spheres, rods, and vesicles—was observed as the degree of polymerization (DP) of the second block increased and the solid content was raised (Fig. 9). The all-PIL nanoparticles

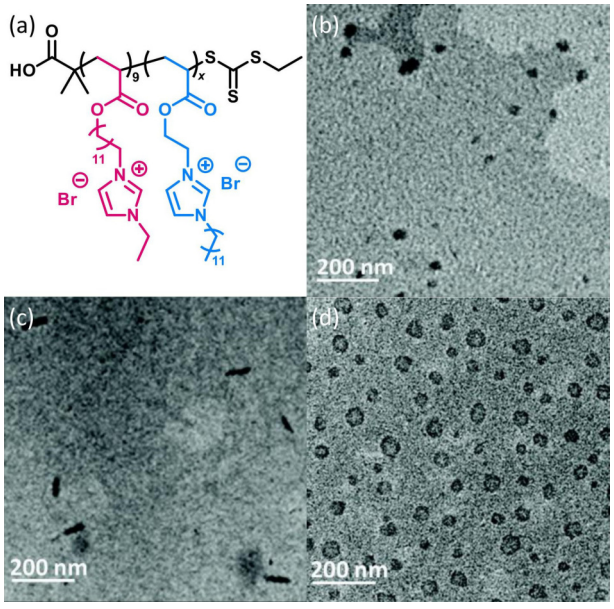

Figure 9 (a) Molecular structure of PADEIBr$_9$-*b*-PAEDIBr$_x$. TEM images of all-PIL block copolymer: (b) spherical nanoparticles (D9-E200-25), (c) rod-like nanoparticles (D9-E600-25), and (d) non-spherical vesicles (D9-800-25) obtained by chain extension of PADEIBr9 with AEDIBr at 25 wt.% solid content [56]. Reproduced with permission from Ref. [56], © Royal Society of Chemistry 2021.

combine the high ionic conductivity of ionic liquids with the processability of polymers, making them promising for potential applications in energy storage (e.g., battery electrolytes) and catalytic supports, among other fields [56].

Besides RAFT-PISA, CMR-PISA is also a common method for the preparation of PILBCPs. In 2016, Detrembleur's group used one-pot CMR-PISA and synthesized an amphiphilic double PILBCPs poly(N-vinyl-3-ethylimidazolium bromide)-*b*-poly(*N*-vinyl-3-octylimidazolium bromide) (PVEtImBr-*b*-PVOcImBr) in aqueous phase under mild conditions (30 °C). By adjusting monomer concentration and polymerization conditions, precise control over the molecular weight, dispersity, and nanoparticle size of the BCPs were achieved, resulting in spherical nanoparticles. Unique "rice-shaped" morphologies could also be obtained at low temperatures by tuning the degree of polymerization. The resulting nanoparticles exhibit high surface charge and long-term stability (maintaining dispersion for months), showing promising potential for applications such as antimicrobial coatings, aqueous catalytic nanoreactors, and ionic conductive materials [35].

In order to reinforce the properties of the material, in 2017, they synthesized amphiphilic BCPs via a one-pot CMR-PISA process in water. The first block, poly(N-vinyl-3-triethylene glycol-imidazolium bromide) (PVTEGImBr), is hydrophilic and provides ionic conductivity, while the second block, composed of a copolymer of N-vinyl-3-ethyl-imidazolium bromide (VEtImBr) and a fluorinated IL monomer 1H,1H,2H,2H-perfluorooctyl-imidazolium bromide (VFImBr), is hydrophobic and contributes mechanical strength. The PDI and TEM images are presented in Fig. 10 together with the former work. The introduction of

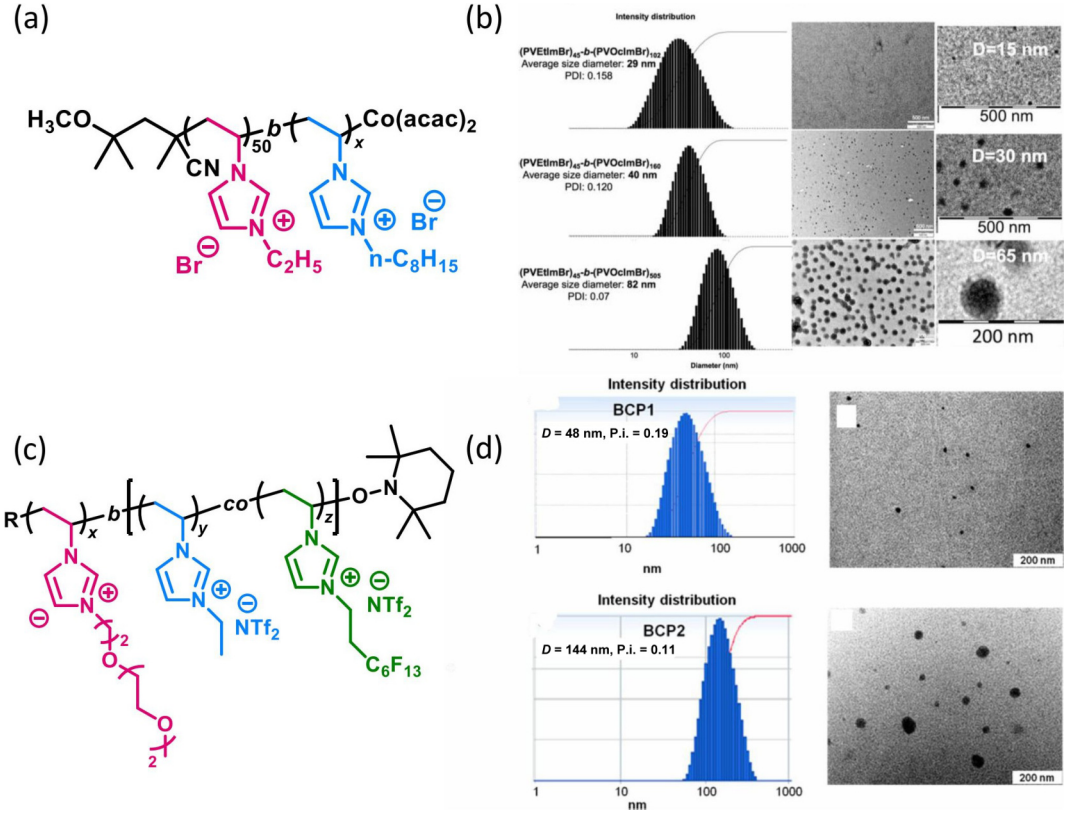

Figure 10 (a) Molecular structure of PVEtImBr-b-PVOcImBr. (b) DLS data and TEM images of some representative BCPs. Reproduced with permission from Ref. [35], © Wiley-VCH GmbH 2016. (c) Molecular structure of PVTEGImBr-*b*-P(VEtImBr-*co*-VFImBr). (d) DLS data and TEM images of two representative BCP. Reproduced with permission from Ref. [57], © American Chemical Society 2017.

fluorinated IL monomer enhances the stability over a large electrochemical window (0–4.8 V versus Li^+/Li). Therefore, the fabricated PILBCP demonstrates high mechanical properties (E = 3.8 MPa at 30 °C) and ionic conductivity (σ_{DC} = 3.0 × 10^{-7} S·cm^{-1} at 30 °C under anhydrous conditions), showing its potential for application in high-voltage and high-safety lithium-ion batteries [57].

3.3.1.3 Ion exchange

Ion exchange is an effective method to investigate the influence of counter ions on morphology. The Mecerreyes research group developed a simple one-step method to prepare PIL nanoparticles and applied them as flocculants in water treatment in 2018. PDADMAC, PAA HCl, and PViEtIMBr were synthesized and partial anion exchange resulted in the formation of amphiphilic random copolymers (e.g., [PViEtIm][TFSI]), which self-assembled into spherical structures in water with particle sizes ranging from 100 to 600 nm (Fig. 11). These nanoparticles significantly accelerated the sedimentation rate when used as flocculants [58].

Ion exchange is also a common method for introducing chirality. For example, a work by Vijayakrishna's group in 2017 introduced chiral amino acids into achiral poly(1-vinyl-3-ethylimidazolium bromide) (P[ViEIm]Br) through anion exchange (Fig. 12) to trigger the formation of helical structures—particularly double helices—and explore their application in asymmetric catalysis. The polymeric precursors were first dissolved in double distilled water; by means of a simple anion exchange reaction, optically pure amino acids (L/D-proline, L/D-histidine) were incorporated as counterions into two types of achiral PIL backbones, inducing the formation of helical conformations [59].

3.3.2 Bulk self-assembly

3.3.2.1 Solvent evaporation

Solvent evaporation is a common method to prepare macroscopic materials like conductive materials. For example, the work by Zhu's group in 2016 synthesized a comb-like polymeric PIL, poly[diethylmethylammonium][4-styrenesulfonyl(trifluoromethylsulfonyl)imide] (P[NH122][STFSI]). The PIL consists of flexible side chains bearing dissociable protonated cations ($[NH122]^+$), a relatively rigid backbone, and hydrophobic anions ($[STFSI]^-$). During the self-assembly process (which is realized by a solvent casting method), the rigid polymer backbone aggregates to form a rigid matrix domain, while the flexible side chains and mobile cations organize into continuous, nanoscale ion channels, enabling high proton conductivity under dry conditions. This material achieves a proton conductivity as high as 3.1 × 10^{-4} S·cm^{-1} at 120 °C under anhydrous conditions [60].

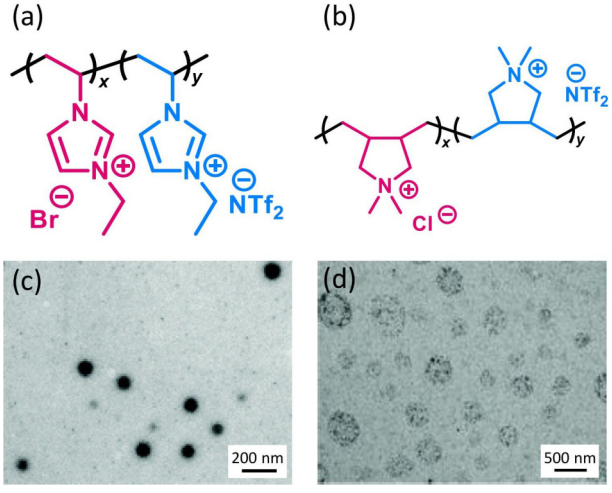

Figure 11 (a) and (b) Molecule structure of PViEtIMBr and PDADMAC after ion exchange. (c) and (d) TEM figures of $PViEtIm_{97.5}TFSI_{2.5}$ and $PDADMAC_{97.5}TFSI_{2.5}$. Reproduced with permission from Ref. [58], © Royal Society of Chemistry 2016.

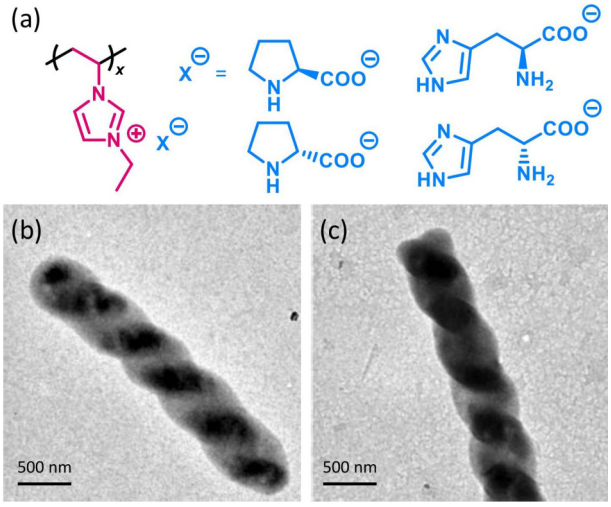

Figure 12 (a) Molecular structures of PILs with chiral anions. Representative TEM figures of (b) poly(ViEIm)-L-his and (c) poly(ViEIm)-D-his. Reproduced with permission from Ref. [59], © Royal Society of Chemistry 2017.

3.3.2.2 Melts

BCPPIL melts can also assemble into various morphologies, not only confined to vesicles or worms, but some bi-continuous phase, which exhibits more interconnection between units. Early works in 2012 by Bailey's group primarily investigated the morphological phase behavior of poly(room-temperature ionic liquid) (poly(RTIL))-containing di-block copolymers in the melt state. Sixteen DOD-*b*-PIL BCPs (where DOD is the hydrophobic block) were synthesized via ROMP. A phase diagram was constructed with the volume fraction of DOD (f_{DOD} = 0.42–0.96) and temperature as variables. Classical BCP phases such as lamellae (Lam), hexagonally packed cylinders (Hex), and body-centered cubic spheres (S_{BCC}) were observed. However, instead of the Gyroid (Gyr) phase between the Lam and Hex regions, a coexistence region of Lam and Hex phases was found. The absence of the Gyr phase suggests that achieving a bi-continuous network structure is particularly challenging in strongly segregated charged/uncharged BCP systems [61].

A similar control strategy was reported in 2019 by the same research group. They prepared a series of PS-*b*-PIL BCPs via ATRP, where the PIL block constituted the majority component (in most cases f_{PIL} > 0.5). The researchers investigated the self-assembly behavior by varying the PIL volume fraction and modifying the alkyl side chains. In contrast to the findings by Scalfani et al., they successfully observed the Gyr phase in PS-*b*-BuPIL, albeit coexisting with the Hex phase. Unlike the methyl-substituted BCPs, which is notoriously sensitive to segregation strength, the more hydrophobic n-butyl substitution significantly reduced the segregation strength (χN) between the PS and PIL blocks, enabling the formation of the gyroid phase. This finding provides important guidance for the

design of PIL-based materials targeting the gyroid morphology for transport applications [34]. Phase diagrams of the above two works can be seen in Fig. 13 (the diagram of PS-*b*-PIL only include BuPIL, a representative BCP).

In fact, studies on both PIL BCPs and conventional BCPs [62–65] have revealed a consistent phenomenon: as the volume fraction (f) of the majority block increases, a morphological transition from Lam to bi-continuous phases (though sometimes unattainable due to specific constraints), to Hex, and finally to Spheres (S) is typically observed. This distinctive trend is attributed to the superior formation of low-orderliness morphologies. The Gyr phase, due to its stringent requirements for chain packing and interfacial curvature, possesses a higher degree of orderliness compared to the Lam and Hex phases, consequently resulting in a higher energy barrier for its formation. This explains its narrow stability window and occasional absence. Among numerous reports, adjusting the volume fraction remains the most common and direct strategy for morphology control, allowing the observation of gradual morphological evolution across a continuous compositional range. Besides, the segregation strength (χN) is also a key factor influencing morphology. Here, N represents the molecular weight, and χ represents the compatibility. Generally, a larger molecular weight leads to a larger periodic size (d) of the self-assembled nanostructures and a higher order-disorder transition temperature (T_{ODT}). When χ is large, the chain segments hardly interpenetrate, and the morphological transitions become more direct (the gyroid phase window narrows or even disappears because its interface with non-constant curvature incurs a high energy penalty under strong segregation strength). In PIL BCP systems, χ plays a dominant role and has a greater influence. This explains why in the work of Bailey's group, simply replacing the methyl group with an n-butyl group enabled the observation of the previously undetected gyroid phase. Specifically, the hydrophobicity of the n-butyl group reduces the χ value, lowering the segregation strength and allowing the gyroid phase to form. In contrast, an n-hexyl group makes the χ value too low, resulting in only microphase separation without long-range order [34]. This demonstrates that the precise control of bi-continuous phases is highly challenging and remains a crucial problem to be solved.

More recent research by Lessard's group in 2022 focuses more on the conductivity application of the bi-continuous phases. They investigated the role of 1,2,3-triazolium-based ionic liquid BCPs in solid-state electrolytes. By combining RAFT polymerization with click reaction, the researchers synthesized PS-*b*-P(VB-Me-TGME-TFSI) and found that it self-assembled into a hexagonally packed cylindrical microphase-separated structure in a melt state. This structure facilitates ion transport, enabling its use as a dielectric layer in Metal–Insulator–Metal (MIM) capacitors, where it exhibits prominent electrical double-layer capacitive behavior and high-frequency response capability. These properties suggest potential applications in flexible electronics and organic thin-film transistors (OTFTs) [36].

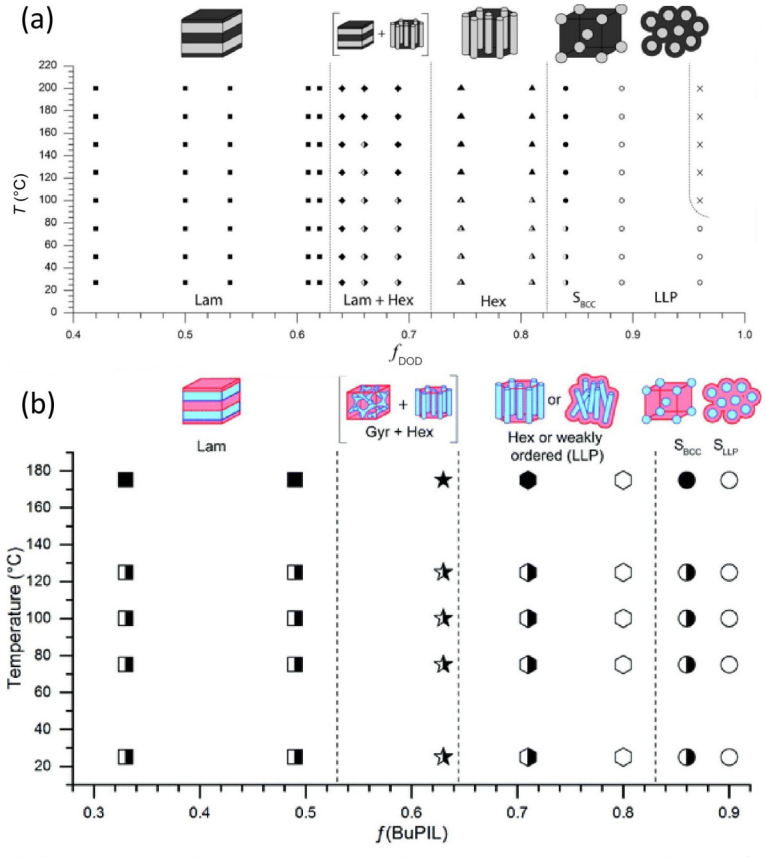

Figure 13 (a) Phase diagram of morphologies observed in the imidazolium-based alkyl–ionic copolymer melt system, where semifilled and open circles represent regions of poorly ordered structures, while cross symbols depict the disordered regio. Reproduced with permission from Ref. [61], © American Chemical Society 2012. (b) Phase diagram of phase separating, n-butyl-substituted PS-PIL BCPs with respect to volume fraction of the PIL component, where filled data points represent highly ordered samples, and half-filled data points represent samples that ordered upon reaching an appropriate annealing temperature and remained ordered in that phase upon cooling, while open data points represent weakly ordered samples. Reproduced with permission from Ref. [34], © Royal Society of Chemistry 2019.

4 Catalytic applications for PILs

PILs exhibit powerful applications across numerous fields, such as sensing materials, gels, catalysis, solid-state electrolytes, etc. In this section, we focus on summarizing the key applications of PILs in the field of catalysis and categorizing the roles they play therein.

The reason PILs can be applied in catalysis is largely due to their nanoscale size, which endows them with unique mass transfer and enrichment capabilities. This has been proved in studies on PIL-based nanoreactors. For example, in 2022, Liu's and Li's group designed a hollow spherical vinylimidazole-based PIL nanoreactor, and its composite with $CoCl_2$ was used for the selective catalytic oxidation of cyclohexane. By comparing the composite catalyst with traditional inorganic catalysts, they found that the nanoscale microenvironment created by the PIL not only enhanced reactant transport but also ensured reaction selectivity and stabilized catalytic sites [66]. In fact, such size effects do not necessarily require capsule-like PIL structures; any nanostructure with a high specific surface area can achieve similar benefits. We will elaborate on the application of PILs in catalysis based on this principle in the subsequent discussion.

4.1 Inherent catalytic functionality of PILs

PILs can be directly employed as catalysts, primarily owing to the functional groups on the ionic liquid monomers. For instance, sulfonic acid groups can confer Brønsted acidity to PILs, enabling them to replace inorganic acids in certain reactions like esterification. In 2016, Wan's and Guan's group synthesized porous PILs containing sulfonic acid groups using Fe_3O_4 nanoparticles as removable hard templates, poly(1-vinyl-3-(3-sulfopropyl) imidazolium hydrogen sulfate, or MPIL, seen in Fig. 14(a)). These PILs exhibited a high specific surface area (43.6 $m^2 \cdot g^{-1}$) and remarkable catalytic activity of esterification of oleic acid with ethanol for biodiesel production (achieving a biodiesel yield of up to 92.6% under optimized conditions). The catalytic activity remained nearly unchanged after six cycles, and their heterogeneous nature facilitated easier product separation [67]. Three years later, Zhang's group synthesized a novel PIL (abbreviated as PIL-S, and detailed structure and synthesis can be seen in Fig. 14(b)) for esterification of acetic acid and butyl alcohol by polymerizing an ionic liquid monomer containing a p-hydroxybenzenesulfonic acid structure with formaldehyde via phenolic condensation. This catalyst exhibited a high acid density (4.5 $mmol \cdot g^{-1}$), achieved a high yield (97.1%) in the esterification of acetic acid and n-butanol, and showed no significant decline in catalytic efficiency after eight cycles [68].

Acidic PILs can function not only as catalysts for esterification reactions but also as substitutes for various other reactions requiring an acidic environment. In fact, the acidic groups are not necessarily attached to the main chain of PILs; they can also exist as counter anion. For instance, Zhou's and Sheng's group synthesized a cross-linked PIL solid acid catalyst (MPM-C_6V-SO_3CF_3-IL, structure can be seen in Fig. 14(c)) with a hierarchical mesoporous-macroporous structure for efficiently catalyzing the alkylation of o-xylene and

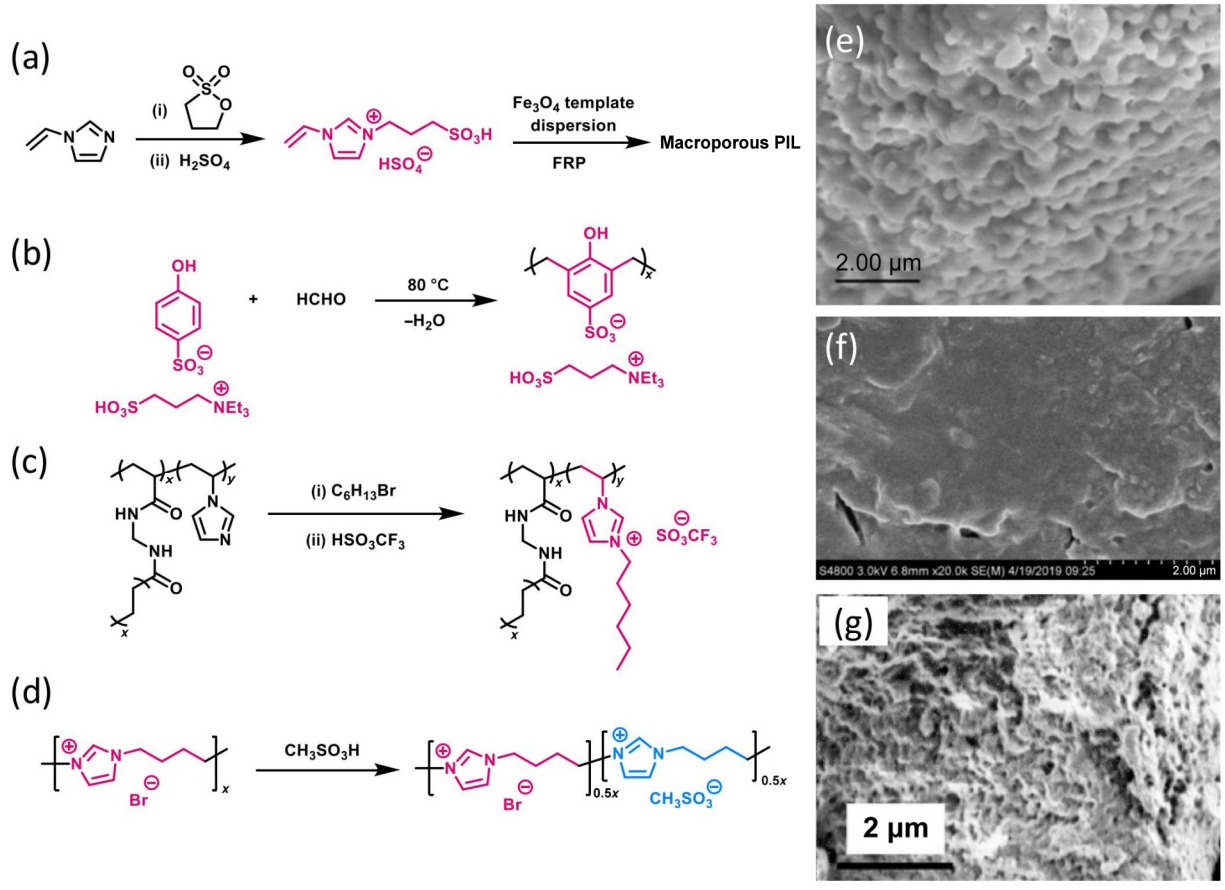

Figure 14 Important synthesis steps of (a) P[VSIM][HSO_4] [67], (b) PIL-S [68], (c) MPM-C_6V-SO_3CF_3-IL [69], and (d) [Pim]$Br_{0.5}(CH_3SO_3)_{0.5}$ [70]. Representative SEM images of (e) MPIL, (f) fresh PIL-S, and (g) MPM-C_6V-SO_3CF_3-IL synthesized in DMF. Reproduced with permission from Ref. [67], © Elsevier Inc. 2016; Ref. [68], © American Chemical Society 2019; and Ref. [69], © Elsevier Inc. 2018.

styrene in 2018. This catalyst exhibited a high specific surface area (103.83 $m^2 \cdot g^{-1}$ in DMF), which is useful in adsorption and outstanding catalytic performance (99.67% yield under optimal conditions). However, its recyclability was relatively poor, with approximately a 50% decline in performance after just four cycles [69].

In another study by Shi's and Xiao's group in 2023, a series of sulfonic acid-functionalized PIL catalysts (a representative structure can be found in Fig. 14(d)) were synthesized to convert biomass feedstocks such as cellulose into levulinic acid (LA) via a one-pot process. The molecular design strategy of this research focused on counterions, modulating both the acidity of the PILs and their cellulose dissolution capacity by varying the counter anions. Under optimal conditions, the reaction achieved a conversion rate of 79.4%. Moreover, the catalyst exhibited high catalytic efficiency for most substrates. Its structural stability was proved by a yield of 68.9% after five reaction cycles [70]. Details of synthesis and SEM characterizations can be found in Figs. 14(e)–14(g).

To achieve a catalyst capable of switching between homogeneous and heterogeneous states via temperature control, Yuan's group designed a 1,2,4-triazolium-based PIL (Ptriaz-C1-I) in 2025 for the synthesis of porous organic cages (POCs, exemplified by CC3R) in methanol. When the temperature is above the upper-critical-solution-temperature (UCST), the PIL dissolves in methanol, forming a homogeneous state in which the catalytic sites are exposed, leading to a significantly accelerated reaction (up to 7.5-fold). Conversely, when the temperature falls below the UCST, the PIL chains collapse and aggregate into a heterogeneous state, where the catalytic sites become encapsulated, thereby slowing down or even halting the reaction [71]. Most studies on PIL catalysts are conducted in organic systems. Therefore, variables such as pH and ion strength in aqueous systems are not considered in the investigation of PIL catalytic performance, while factors like temperature or pressure (in gas-phase reactions) are taken into account.

There is also an important and extensively studied catalytic application of PILs: their use in reactions involving carbon dioxide (CO_2). Some recent studies have involved PIL-catalyzed formylation of amides using CO_2 [72] and the conversion of CO_2 into dimethyl carbonate [73], etc. Among all reactions involving CO_2, cycloaddition of propylene oxide is the most studied and well developed (Fig. 15(a)). Early research proposed that PILs absorb CO_2 through two primary mechanisms: physical adsorption and chemical adsorption. The former involves the reversible capture of CO_2 molecules via intermolecular forces (such as electrostatic interactions between cations and anions) [74], while the latter occurs when specific groups in the IL react with CO_2 to form decomposable carboxylate salts [75].

Research on the use of PILs for catalyzing CO_2 cycloaddition has already been initiated in earlier stages. In 2011, Xiong's group synthesized a highly cross-linked PIL using 4-vinylbenzyl-tributylphosphonium chloride and the cross-linker ethylene glycol dimethacrylate (Fig. 15(b)). They form spherical nanoparticles with average size of 10–30 nm during the process of crosslinking in methanol. For catalytic application, under optimal conditions, both the conversion and selectivity reached 100%, and the catalyst could be recycled six times without significant loss of activity. However, mechanism of the whole process was not studied in this work [76].

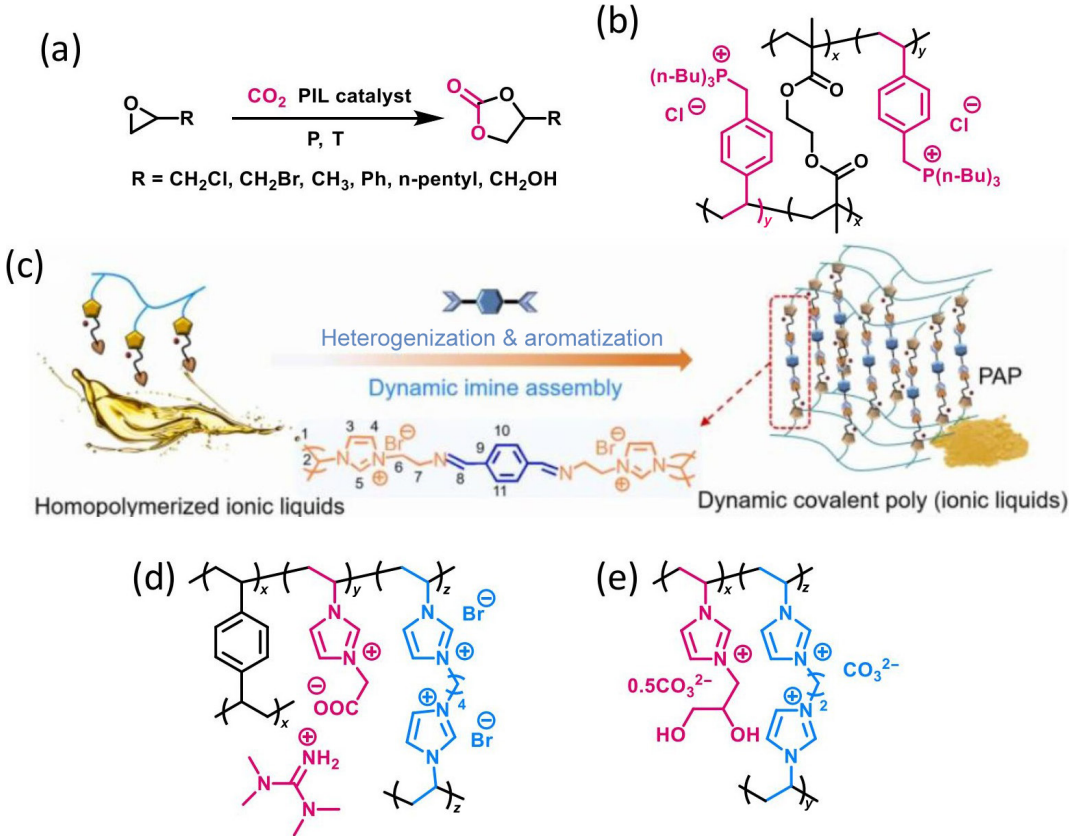

Figure 15 (a) The reaction of CO_2 cycloaddition. (b) Molecular structure of poly(4-vinylbenzyl-tributylphosphorous chloride) [76]. (c) Schematic illustration for the heterogenization and aromatization of homopolymerized ionic liquid. Reproduced with permission from Ref. [77], © Elsevier Inc. 2023. Molecular structure of (d) P-DBTMGH [78] and (e) P-HB-2OH-CO_3 [79].

This topic is still prevalent in recent years and progress has been made. Shi's and Yi's group developed a simple and green method to convert homogeneous PILs into porous, aromatized heterogeneous catalysts (Fig. 15(c)) in 2023. The aromatized moiety activates CO_2 and enhances its reactivity. Furthermore, through simulation and calculation of the activation energy, they demonstrated that the catalytic activity of the PIL increases with the enhancement of aromaticity. Importantly, in this work, even when the CO_2 concentration was reduced to 15%, a yield of 92% and a selectivity of 99% were still achieved, demonstrating the industrial potential of this PIL [77].

Researchers also focused on the catalysis of the cycloaddition of low-partial-pressure CO_2 (15% CO_2 + 85% N_2). Guan's group developed a heterogeneous catalyst in 2024: guanidine-functionalized basic binuclear PIL (GB-PIL) (Fig. 15(d)) with epoxides to form cyclic carbonates under mild conditions, without the need for any co-catalyst or solvent. The basicity of the guanidine group and the high bromide ion concentration provided by the binuclear structure synergistically catalyze the reaction. According to the experiments, a 5.4 wt.% catalyst loading can achieve a 96% yield and a 99% selectivity under suitable conditions (2.0 MPa, 15 vol.% CO_2 + 85 vol.% N_2, 100 °C 4 h) [78].

The following year, the same research group further explored the catalysis of low-concentration CO_2 by designing and synthesizing a multifunctional PIL catalyst with high-density nucleophilic sites and CO_2 adsorption sites (P-HB-2OH-CO_3) (Fig. 15(e)). This catalyst features both dihydroxy and carbonate bifunctional sites. Like the previous work, the carbonate groups provide basicity, while the dihydroxy groups activate the oxygen atom of the epoxide to promote ring-opening, enabling synergistic catalysis between the two functional groups. Under reaction conditions identical to those in the previous work, the yield achieved by this catalyst reached 95% [79].

For the catalysts in the three aforementioned studies, their CO_2 adsorption capacities are critical, measuring 0.081 (though characterized as pore volume), 13.05, and 15.24 $cm^3 \cdot g^{-1}$, respectively. They demonstrate relatively high active reaction sites, which contribute to their good catalytic performance.

Although the specific mechanisms of the CO_2 cycloaddition reaction catalyzed by PILs vary across different studies, they share several common features. The overall cycloaddition process consists of three steps: activation of the epoxide, nucleophilic attack/ring-opening, and CO_2 insertion. Among these, ring-opening and insertion are the two key steps. As research advances, multi-site catalysts have garnered increasing attention due to the synergistic catalysis between their distinct sites, which significantly enhances catalytic efficiency. The catalyzing mechanism of GB-PIL can be seen in Fig. 16 as a representative example. Owing to the unique

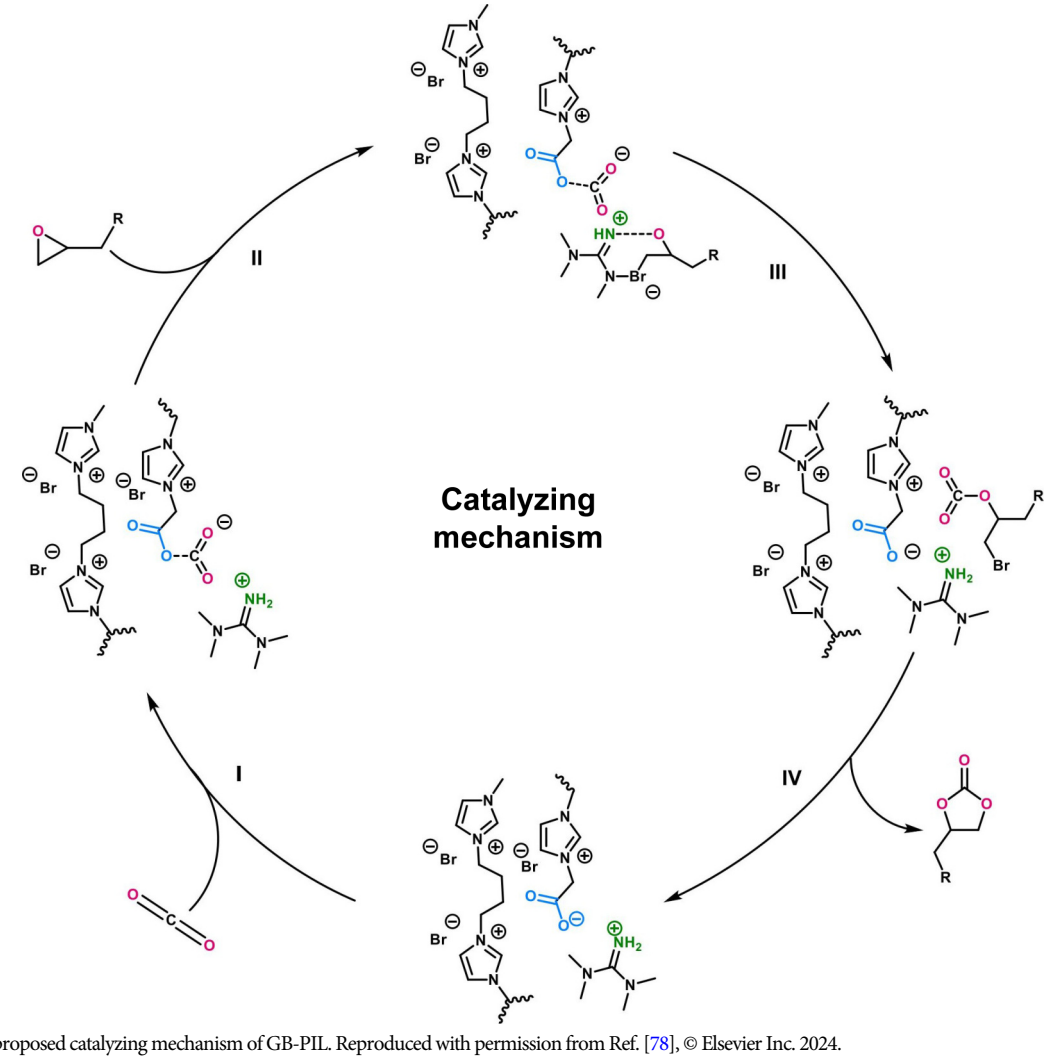

Figure 16 The proposed catalyzing mechanism of GB-PIL. Reproduced with permission from Ref. [78], © Elsevier Inc. 2024.

properties of PILs, these catalysts exhibit lower requirements for CO_2 concentration. What's more, compared to conventional homogeneous catalysts for this reaction like tetrabutylammonium bromide (TBAB) or potassium iodide (KI) (nucleophilic reagents) and halides of zinc, cobalt, aluminum, etc. (Lewis acids), recent studies are shifting towards heterogeneous catalysis, which not only facilitates the subsequent separation of catalysts but also holds potential for industrial applications.

4.2 Catalyst carriers

The application of PILs as catalysts is relatively limited, primarily because the catalytic conditions they provide are mainly derived from their functional groups (e.g., acidity from carboxyl groups, basicity from amino groups, etc.), while their polymeric backbone rarely participates in catalysis. For this reason, research on combining PILs with other materials to form composites has grown significantly in recent years. In this section, we will focus on studies involving PILs self-assembled and loaded with metal, PILs serving as components to form metal-organic framework (MOF) materials with metal, and metal as centers stabilized by PILs.

4.2.1 Self-assembled PILs as supports for metals

Both metal nanoparticles and metals ions can be carried by self-assembled PILs to demonstrate catalytic abilities.

4.2.1.1 Metal nanoparticles

One method for immobilizing metal particles involves the self-assembly of PILs, which tightly anchor the metal nanoparticles to the PIL framework through coordination, ion exchange, adsorption, and other interactions. The key advantages of this approach include higher and more stable specific surface area of metal nanoparticles, the potential synergistic catalytic capability between the PIL and the metal, as well as the composite typically serving as a heterogeneous catalyst, enabling easy separation. These benefits distinguish PIL/metal composites from conventional metal particles.

Some materials are designed with PILs as the central component, which first self-assemble into nanostructures and are then composited with metal NPs for catalysis. Palladium (Pd), as a common catalyst in organic reactions, plays an irreplaceable role in numerous coupling reactions and many other reactions [80–82]. Therefore, many researchers have explored the integration of Pd with PILs in the recent decade. For example, in 2015, Yuan's group designed core–shell structured PIL@SiO_2 nanospheres with the help of surfactant cetyltrime-thylammonium bromide (CTAB) for supporting Pd nanoparticles. They used poly(vinylimidazolium)-based PIL as the core and applied a silica coating as the shell (Fig. 17(a)). Pd nanoparticles were immobilized within the PIL core via ion exchange followed by reduction. This amphiphilic design enabled the selective oxidation of aromatic alcohols to proceed in an aqueous phase with exceptionally high conversion (> 99%) and selectivity (100%) [83].

In 2016, Groppo's group investigated the stabilizing effect of PILs as supports for palladium nanoparticles and their influence on catalytic performance, particularly chemoselectivity. They synthesized the polymer/Pd composite by hydrogen reduction, obtaining Pd NPs smaller than 2 nm (Fig. 17(b)). They found that PIL-supported Pd exhibited exceptionally high selectivity, which was primarily attributed to the ionic environment provided by the PILs, leading to enhanced stability of Pd. This work offers new insights for designing highly selective hydrogenation catalysts under mild conditions [84].

Researchers also paid attention to electron effects such as the selective hydrogenation of α,β-unsaturated carbonyl compounds and dienes. Dupont's group systematically investigated the influence of PIL as a support on the structure, electronic properties, and catalytic performance of Pd nanoparticles in the above reaction. They found that the synergistic effect between PIL and IL significantly enhanced catalytic activity and stability. By comparing the performance of various catalysts, they concluded that the sputtering method combined with a PIL/IL hybrid support could produce Pd NPs with high Pd(0) content, small size, and high dispersion, exhibiting excellent catalytic performance [85].

Ghomi's group noticed the potential of the combination of carbohydrate polymers with PILs, so they utilized allylated chitosan and a polymerizable ionic liquid ([MEVIm]Br) to form a cross-linked ionic biopolymer through free radical copolymerization in 2023, developing a biodegradable chitosan-based PIL composite material (CS-PIL) (Fig. 17(c)). This material served as a support for stabilizing Pd nanoparticles, constructing a highly efficient and recyclable heterogeneous nanocatalyst (Pd@CS-PIL). They achieved highly dispersed and stable loading of Pd NPs, with the catalyst demonstrating super activity, high selectivity, and excellent recyclability [86].

The oxidation of benzyl alcohol is a highly important reaction in chemical industry. In a recent study in 2025, Song's group developed a polymerizable IL based on 3-benzyl-1-vinylimidazolium, which was copolymerized with different amounts of ethylene glycol dimethacrylate (EGDMA) to form a PIL. Using a chemical reduction method, they successfully loaded palladium nanoparticles (Pd NPs) onto the PIL, creating a uniformly dispersed porous structure with Pd NP sizes ranging from 1.5 to 3.5 nm. Under the reaction conditions of 0.1 g of 1% Pd/PIL catalyst, 110 °C, 4 MPa O_2, and 4 h, they achieved a benzyl alcohol conversion rate of 82.16% with 100% selectivity toward benzaldehyde. Their DFT calculations further revealed that the palladium clusters exist as Pd_6 species, which was identified as a highly active and stable structure [87].

Apart from Pd, gold (Au) is also a very common catalyst [88–90], which is why numerous studies have combined Au with PIL to improve its catalytic performance. In 2017, Moghaddam's group developed a gold nanoparticle catalyst supported on magnetic PIL by using Fe_3O_4@SiO_2 as the magnetic core, functionalizing it with 3-(trimethoxysilyl)propyl methacrylate, and copolymerizing it with 1-vinylimidazole, 1-ethyl-3-vinylimidazolium bromide, and a cross-linking agent (Fig. 17(d)). This catalyst was used for the efficient and selective reduction of nitroarenes, enabling easy recovery and reuse. Compared to conventional inorganic material-supported AuNPs composites like mesoporous TiO_2@AuNPs, this catalyst exhibited higher gold loading capacity (exhibiting a 17-fold increase) and superior catalytic efficiency (a 5 time increase in reaction rate) [91].

In fact , PILs show an excellent coordination ability with various transition metals. Song's group synthesized copolymers containing imidazolium groups (e.g., P([EVIm]Br-EGDMA)) for the co-loading of Au and Ru species in 2019. These materials are designed for catalytic wet air oxidation (CWAO) of ammonia. The support material is constructed from spherical nanoparticles as primary building blocks, which interweave to create a three-dimensionally crosslinked framework. Au exhibits larger aggregate sizes compared

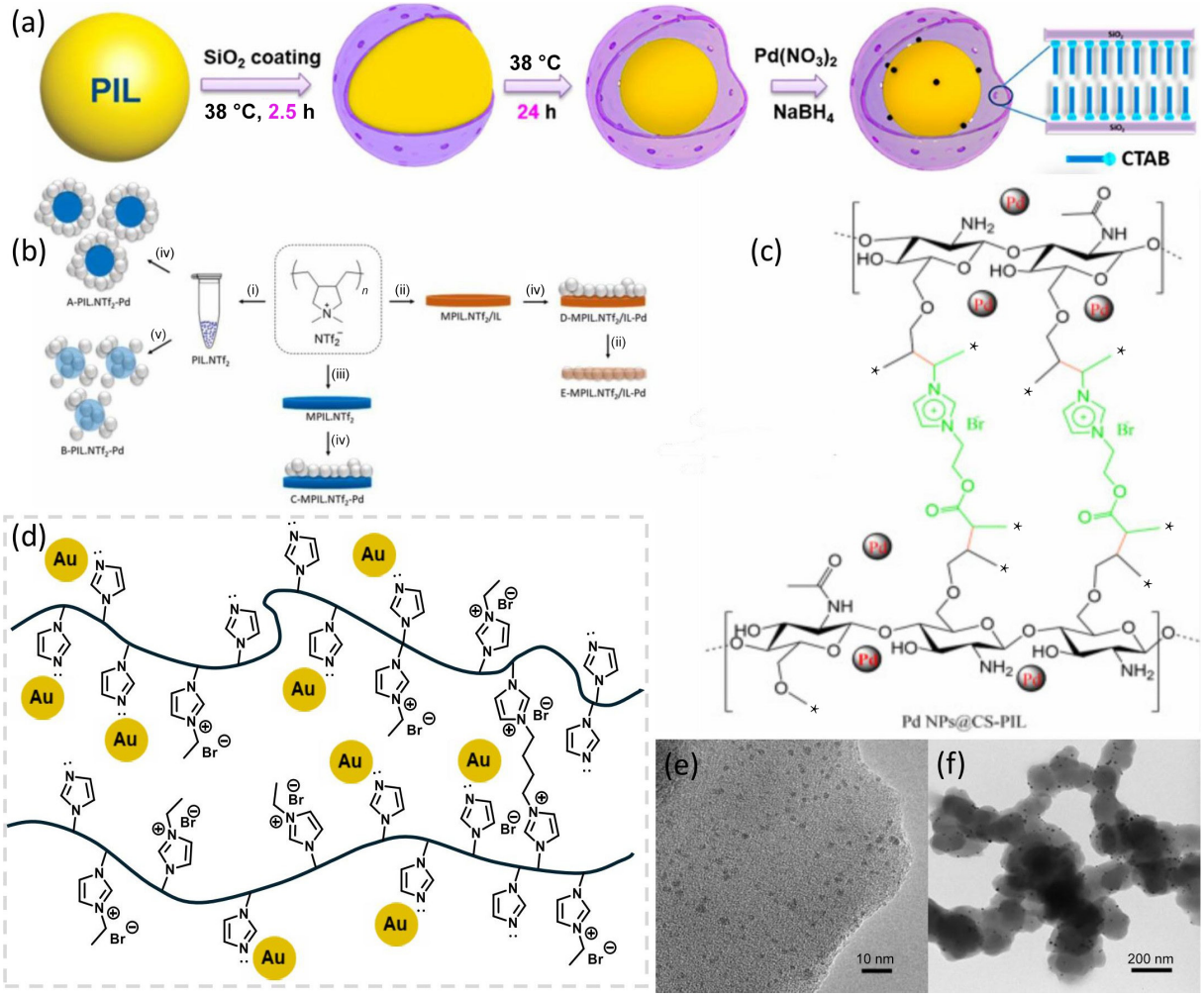

Figure 17 (a) Schematic illustration of the synthetic route to the PIL@SiO_2-Pd nanoreactor. Reproduced with permission from Ref. [83], © American Chemical Society 2014. (b) Pathways to prepare supports and Pd NPs catalyst ((i) = maceration; (ii) = acetone, BMI.NTf_2, moulding in petri plate; (iii) = acetone, moulding in petri plate; (iv) = sputtering deposition; (v) = $Pd(OAc)_2$, methanol, 75 °C, 4 bar H_2). Reproduced with permission from Ref. [85], © Elsevier Inc. 2018. (c) Schematic structure of Pd@CS-PIL. Reproduced with permission from Ref. [86], © Elsevier Inc. 2023. (d) Schematic structure of Au@PIL. Reproduced with permission from Ref. [91], © Wiley-VCH GmbH 2017. TEM images of (e) Ru/PILs-NTf_2 and (f) Au/PILs-NTf_2. Reproduced with permission from Ref. [92], © Elsevier Inc. 2019.

to Ru, likely attributable to its multifaceted interactions with the support matrix: Au can coordinate with both the –COO– groups of EGDMA, the –S=O moieties of –NTf_2, and the imidazolium rings, whereas Ru is primarily restricted to interactions with the imidazolium rings alone. This differential binding capacity results in more robust Au stabilization and consequently larger particle formation. In the catalytic reaction, Au demonstrated a conversion rate of 65.8% with 99% selectivity, while Ru achieved higher conversion at 86.5% but slightly lower selectivity (95%) [92]. TEM characterizations can be found in Figs. 17(e) and 17(f).

This research group recently achieved a breakthrough in loading Au nanoparticles (AuNPs) onto PILs. To efficiently convert 5-hydroxymethylfurfural (HMF) into dimethyl 2,5-furandicarboxylate (FDMC), they developed a polymerizable ionic liquid, $[Dimbv]Cl_2$, and performed ion exchange to replace Cl^- with NTf_2^-. Similar to the Pd-loading approach described in reference [87], they copolymerized IL and EGDMA in different ratios and loaded AuNPs via chemical reduction. Under the reaction conditions of 0.15 g of 2% Au/PILs-Tf_2N catalyst, 120 °C, 2 MPa O_2, 0.75 equivalents of CH_3ONa, and 12 h, they achieved 96.41% conversion of HMF and 100% selectivity toward FDMC. They also employed DFT calculations to propose a plausible reaction mechanism [93].

Based on the aforementioned studies, it is evident that the predominant method for immobilizing metals onto PILs is chemical reduction, with only a limited number of cases utilizing sputtering deposition. This is because metal NPs deposited by the sputtering method can only be loaded on the surface of PIL, resulting in poor binding. In contrast, the chemical reduction method allows metal NPs to be more uniformly dispersed on PIL with better binding. However, although the binding is improved, the chemically reduced metal NPs have an uneven size distribution, which may lead to smaller NPs aggregating onto larger ones, thereby reducing the specific surface area and decreasing catalytic efficiency. This is a key reason why the service life of PIL@metal NP materials is shorter than that of conventional industrial catalysts. This can be illustrated by the metal leaching rate. For example, in the work of reference [93], the initial loading rate of AuNPs was 1.4967%, which decreased to 1.2650% after five cycles—representing a decrease of approximately 15.5%. As a result, it is imperative to develop a novel strategy for loading metals onto PILs.

PILs exhibit strong binding affinity with most transition metals (such as cobalt, copper, nickel, etc.) and have found corresponding applications in the catalytic fields associated with each metal. In recent years, Cu composites have also been synthesized and applied in various fields. To be more specific, in the work of Yuan's group in 2023, single component assembly of PIL into homopolymer dense spheres, worm-like structures and nanovesicles (NVs) with tunable sizes (50–120 nm) and shell thicknesses (15–60 nm) was achieved. Ultra-small copper nanoparticles (CuNPs, 1–3 nm) were *in situ* loaded into the PIL nanovesicles to form PIL/Cu composite materials. These composites exhibited high selectivity for C_1 products (e.g., CH_4) in the CO_2 electroreduction reaction (CO_2ER), achieving a 2.5-fold enhancement compared to unmodified CuNPs [94].

4.2.1.2 Metal ions

The binding modes of metal ions and metal NPs to PILs are distinct. Metal NPs are typically encapsulated or embedded within PILs through spatial effects such as nanoconfinement and steric hindrance, whereas metal ions are primarily bound via chemical bonds, such as coordination bonds. These ions are anchored onto the polymer backbone in an atomically dispersed manner, resembling the concept of single-atom catalysis (although they are not strictly individual atoms). There has been plenty of work on this topic recently. For example, Yuan's group synthesized a series of poly(4-alkyl-1-vinyl-1,2,4-triazolium)-based PILs with varying substituents in 2016, explored their loading capacities of transition metals ions like Co^{2+}, Ni^{2+}, and Cu^{2+}, and compared the loading amounts with imidazole analogues (as shown in Fig. 18(a)) [95].

To apply the loaded ion metals to real catalyzed reactions such as the aerobic C–H/C–H coupling of aromatic compounds under ambient conditions, Wang's and Zhou's group synthesized PDMPyPs (a copolymer of N-propane sulfonate-4-vinylpyridine, maleic anhydride and divinylbenzene) via free-radical copolymerization, with Pd(II) loading achieved through oxygen coordination (Fig. 18(b)). The system's stability is primarily maintained by carboxyl groups. The hybrid Pd^{II}@PDMPyPs exhibit catalytic activity toward. The biphenyl yield reached 15.0% (selectivity: 98.5%, turnover number: 62), surpassing conventionally used homogeneous palladium acetate catalysts. The micrometer-

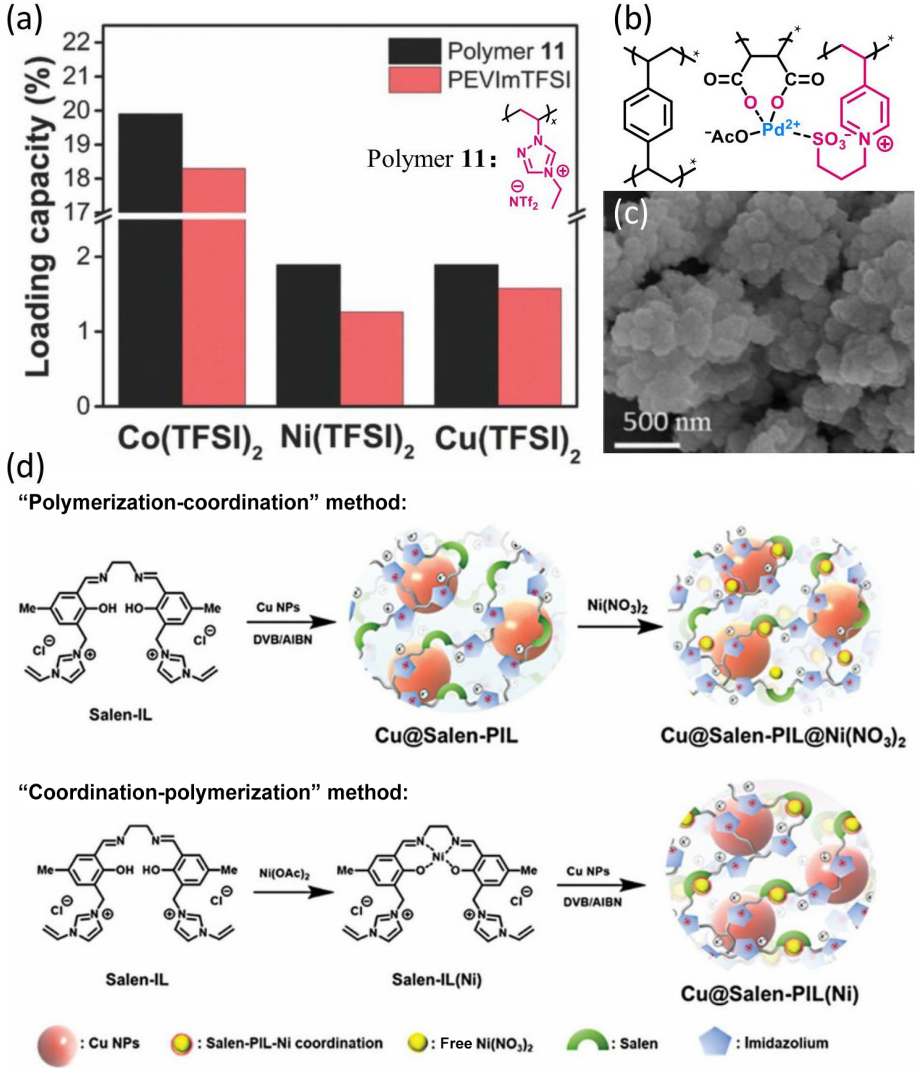

Figure 18 (a) Loading of Co/Ni/Cu ions in polymer 11 (black) and PEVImTFSI (red) at a fixed mixing molar ratio of metal/monomer unit ~ 2. Reproduced with permission from Ref. [95], © Wiley-VCH GmbH 2016. (b) Molecular structure of Pd^{II}@PDMPyPs [96]. (c) SEM image of Pd^{II}@PDMPyPs. Reproduced with permission from Ref. [96], © Elsevier Inc. 2018. (d) The synthetic diagram of Cu@Salen-PIL, Cu@Salen-PIL@$Ni(NO_3)_2$, and Cu@Salen-PIL(Ni) with different synthetic methods. Reproduced with permission from Ref. [98], © Wiley-VCH GmbH 2024.

scale aggregates shown in the figure are composed of numerous 20–30 nm primary particles (Fig. 18(c)). This hierarchical structure provides the high surface area desirable for catalytic support applications [96].

The introduction of metal ions can not only promote catalyzing abilities, but they also present the potential of inducing self-assembly. Li's and Liu's group proposed and systematically studied a cobalt-based PIL catalyst in 2024 for the highly efficient and selective oxidation of cyclohexane to KA oil (cyclohexanone and cyclohexanol) without additional initiators. They used poly(N-vinylimidazole)-based PIL as the framework and coordinated it with $CoCl_2$ to form Co-PIL. In this hybrid catalyst, hydrogen bonding and electrostatic interaction provided stability. By varying the Co content in the Co-PIL, the researchers observed spherical aggregates, and a potential porous structure was identified. The catalytic performance far surpassed that of traditional metal salts. By synergistically regulating the metal centers and the PIL microenvironment, they established a controllable catalytic strategy with a certain degree of substrate versatility [97].

The same year, Xu's group noticed the feasibility of loading multiple metal, so they proposed a copper-nickel bimetallic electrocatalyst based on PIL, which significantly enhanced the performance of CO_2 electroreduction to C_2^+ products by stabilizing high-valence Cu(I) sites and constructing Cu–Ni interfaces. Cu@Salen-PIL@Ni$(NO_3)_2$ and Cu@Salen-PIL(Ni) were synthesized via "polymerization–coordination" and "coordination–polymerization" methods (Fig. 18(d)), respectively. They found that the synergistic effect between the Cu–Ni interface and the tandem catalytic system is key to improving the selectivity and activity toward C_2^+ products. They further investigated the influence of the Ni species' forms on the catalytic selectivity, and they found that after electrolysis, Ni in Cu@Salen-PIL@Ni$(NO_3)_2$ exists in both metallic and oxide forms, whereas in Cu@Salen-PIL(Ni), it remains consistently in the form of a complex. The former promotes C–C coupling and suppresses CH_4 production due to the Cu–Ni interface, while the latter, due to the isolated Ni sites, has a higher probability of competing reactions, resulting in relatively lower selectivity [98].

By comparing the work on PIL-supported metal NPs and metal ions, we can discover that the former focuses more on noble metals (e.g., Pd, Au), while the latter also includes abundant metals (e.g., Ni, Co). This is because, compared to the excellent stability of noble metals, abundant metals are highly susceptible to oxidation, leading to the formation of oxides during synthesis, which diminishes their catalytic performance. Moreover, from a synthetic perspective, obtaining Ni, Co, and other metal NPs via chemical reduction requires strong reducing agents and strictly anhydrous/oxygen-free conditions, making the process undoubtedly more demanding than the reduction of noble metals. However, the ferromagnetic properties of these metals hold significant application potential. If successfully supported on PILs as NPs, it might be possible to modulate their catalytic performance by altering the electromagnetic environment. To the best of our knowledge, no such work has been reported yet, likely due to the considerable difficulty in overcoming the above challenges.

4.2.2 *PILs as components of MOFs*

MOFs are composed of organic linkers and metal ions or clusters, and are characterized by their high specific surface area, porosity, high designability, and high structural order. These properties make them excellent candidates for heterogeneous catalysts [99–101]. However, the functionality of conventional MOF materials is often limited, as they typically possess only Lewis acid sites for catalysis, and some MOF structures exhibit poor hydrothermal stability. To address these issues, researchers have attempted to incorporate PIL into MOF materials (PIL@MOF). The cationic and anionic structure of PIL introduces additional functional sites into the composite material, such as nucleophilic sites (e.g., halide ions).

Literature indicates that simply incorporating ILs into MOFs can generate strong internal stress between the two components [102–104], leading to the collapse of the entire MOF structure or chemical incompatibility, resulting in the blockage of the MOF's porous structure by PIL chains. Therefore, early research on PIL@MOF materials focused more on achieving an ordered structure. For example, the Zhuang's and Wang's group utilized a composite of ZIF-67 and PIL (poly(1-vinyl-3-ethylimidazolium tetrafluoroborate)) in 2017 to prepare a high-performance oxygen reduction reaction electrocatalyst composed of cobalt nanoparticles coated with ordered nitrogen-doped porous carbon (Co@O-NPC). Compared to the Co@DO-NPC catalyst obtained traditionally by carbonizing pure ZIF-67, Co@O-NPC possesses an ordered carbon layer. Through molecular dynamics simulations, they demonstrated that the ordered carbon layer (graphene model) is more conducive to the diffusion of O_2 and H_2O than the disordered carbon layer (amorphous carbon model), thereby explaining why Co@O-NPC exhibits superior catalytic performance [105].

In fact, more recent work about PIL@MOF focuses more on the catalytic application in the conversion of CO_2. This is because the high specific surface area of MOFs enables the enrichment of CO_2, while the strong CO_2 affinity of PILs results in a high local CO_2 concentration, which facilitates the catalytic process. Moreover, the Lewis acid sites on MOFs and the catalytic sites on PILs can synergistically catalyze the reaction. Compared to simply loading metal nanoparticles or metal ions, PIL@MOF exhibits significant advantages in both the dispersion and stability of catalytic sites.

Jiang's group developed a strategy to confine imidazolium-based PIL (poly(1-vinyl-3-ethylimidazolium bromide)) within the pores of the metal–organic framework MIL-101 via *in situ* polymerization in 2018, successfully constructing a PIL@MIL-101 composite (Fig. 19(a)). This composite efficiently catalyzes the cycloaddition of CO_2 with epoxides under cocatalyst-free and mild conditions (atmospheric pressure, ≤ 70 °C). Its exceptional performance originates from the synergistic effect between the MOF and the PIL: the MOF is responsible for enriching CO_2 and providing Lewis acid sites (Cr^{3+}), while the PIL provides nucleophilic bromide anions (Br^-) as Lewis base sites. The incorporation of the IL and the crosslinker DVB resulted in the formation of a three-dimensional network structure after polymerization. Compared to the activities of pure MIL-101 (27%) or the IL monomer (42%), this catalyst achieved a significantly higher activity of 94% without requiring any cocatalyst. Furthermore, the researchers demonstrated a positive correlation between CO_2 capture capacity and conversion efficiency, which explains the reason for the exceptionally high conversion efficiency of this catalyst [106].

Liu's group expanded the structures of MOFs, and tried various Zn based MOFs. For example, they prepared Zn-TPMO$_x$@PIL-C$_n$ [107] by incorporating imidazolium-based PILs with varying alkyl chain lengths into zinc porphyrin-functionalized organosilicas (Zn-TPMO$_x$) via *in-situ* polymerization. Apart from this, PIL-Br$_x$@Zn-

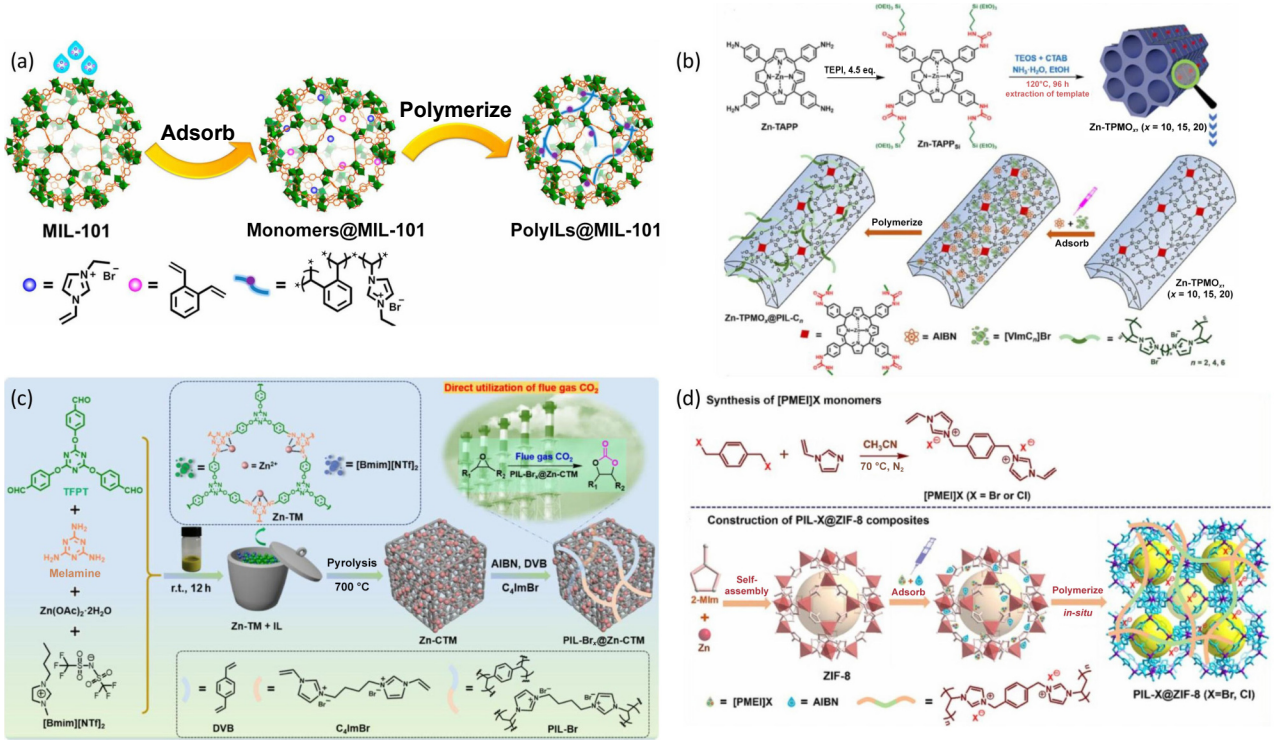

Figure 19 Schematic synthesis routes of (a) PIL@MIL-101 (reproduced with permission from Ref. [106], © American Chemical Society 2018), (b) Zn-TPMO$_x$@PIL-C$_x$ (reproduced with permission from Ref. [107], © Elsevier Inc. 2023), (c) PIL-Br$_x$@Zn-CTM (reproduced with permission from Ref. [108], © Elsevier Inc. 2024), and (d) PIL-X@ZIF-8 (reproduced with permission from Ref. [109], © Elsevier Inc. 2024).

CTM [108] and core–shell PIL@ZIF-8 nanocomposites [109] were also fabricated (the schematic preparation of the above three PIL@MOFs is presented in Figs. 19(b)–19(d) in sequence). Zn-TPMO$_x$@PIL-C$_n$ provided dual hydrogen bond donors and Lewis acid sites (Zn^{2+}), while the PIL contributed nucleophilic Br^- anions and Lewis basic sites. The rest two PIL@MOFs featured similar Lewis acid-base sites and nucleophilic sites. Under solvent-free and co-catalyst-free conditions, they all achieved a yield over 90% with > 95% selectivity for the conversion of CO_2 into carbonate esters under optimal conditions.

For the same reaction, Liao's and Zhao's group discovered the possibility to apply Zr to PIL@MOF. They synthesized UiO-66-NH_2 with an octahedral structure using a conventional hydrothermal method. A PIL shell was constructed on the surface of UiO-66-NH_2 via a two-step method, where the $-NH_2$ groups guided the uniform coverage of PILs, forming a complete core–shell structure. UiO-66-NH_2 provides Lewis acid sites (Zr^{4+}), while the PIL provides nucleophilic sites (Br^-). Under solvent-free and co-catalyst-free conditions, both the yield and selectivity exceeded 99%. However, this catalyst showed limited applicability for the sterically hindered cyclohexene oxide, resulting in a significantly reduced yield (< 5%) [110].

Although research on PIL@MOF composite materials is quite extensive, quantitative computational studies on their binding mechanisms remain limited. Here, we referenced recent research from Song's group [111], who used DFT theoretical calculations to investigate the interactions between imidazolium-based PILs and phenolic compounds, finding that π–π interactions play a significant role. In PIL@MOF materials, the MOF acts as a rigid framework, while the PIL exists as relatively free chains. The interactions between them involve both physical and chemical aspects. The former arises from the confinement effect created by the porous structure of the MOF, where PIL chains are embedded within these channels, adopting specific conformations that enhance the exposure of certain functional groups, thereby improving catalytic performance. The latter involves π–cation interactions, as MOF materials often contain abundant π-systems, and the PILs studied in the aforementioned works are predominantly imidazolium-based cations, enabling strong interactions that ensure chemical stability. Furthermore, experimentally, thermogravimetric analysis (TGA) has been widely employed in these studies to demonstrate the thermodynamic stability of PIL@MOF materials. Compared to traditional pure MOF carriers or polyelectrolytes, the relatively free nature of PIL chains ensures their mechanical flexibility, while their counterions form potential ion channels, facilitating ion transport. Another advantage is that the chemical stability of PIL@MOF enables *in situ* functional group modification.

The PIL@MOF materials in the above studies all possess considerably high specific surface areas, which is directly associated with the ability to adsorb CO_2. Detailed statistics can be seen in Table 2. We can discover from the table data that the specific surface area significantly decreases after PIL composite formation, which serves as important evidence for the genuine formation of an ordered PIL@MOF structure rather than a disordered mixture. In fact, despite the reduction in specific surface area, the composite material still far exceeds that of conventional PILs (the specific surface area of typical PILs usually does not exceed 50 $m^2 \cdot g^{-1}$). Although the composite material has a lower specific surface area than the pure MOF structure, this drawback is compensated by the multi-site synergistic catalysis between the two components—A feature that neither PILs nor MOFs alone can achieve.

PIL@MOF exhibits catalytic performance that is positively correlated with its specific surface area. Turnover number (TON) is

a crucial parameter for measuring the catalytic efficiency of a catalyst. PIL-Br1.0@Zn-CTM achieves a maximum TON of 723 [108], whereas Zn-TPMO$_{20}$@PIL-C$_6$, which has a higher specific surface area, reaches a TON as high as 2811 [107]. This comparison clearly demonstrates a close relationship between TON values and specific surface area. Other key catalytic performance parameters, such as the number of reusability cycles and selectivity, do not show significant differences in the performance of the aforementioned materials. This is because TON is related to the exposure of active sites, which is well reflected by the specific surface area, whereas reusability cycles and selectivity are less directly associated with it.

4.2.3 *PILs attached to center metals as stabilizers*

PILs can also be grafted onto metal NPs as stabilizers, typically forming a core–shell structure. However, to the best of our knowledge, this sort of work is not very widely applied in catalysis. This is because the usual active site of this kind of material is the metal core, which is commonly spherical. Such morphology will result in a low specific surface area, a feature not desirable for catalysts. As a result, PILs are added to enrich the substrates' concentration, which compensates for the relatively low specific surface area to improve catalysis. There is some early and work about this topic. For example, in 2016, Verdugo's and Luis's group developed gold NP–PIL composite (Fig. 20(b)) multifunctional catalytic nanoreactors for one-pot cascade reactions. They constructed a nanocomposite material featuring multiple catalytic active sites and a controllable hierarchical structure. A series of 1-butylimidazole-based PILs were designed to form a stabilizing shell

Table 2 The specific surface area of different PIL@MOF

PIL@MOF	Specific surface area of pure MOF ($m^2 \cdot g^{-1}$)	Specific surface area after the incorporation of PILs ($m^2 \cdot g^{-1}$)	Reference
PIL@MIL-101	3603	2462	[106]
Zn-TPMO$_{20}$@PIL-C$_6$	831	493	[107]
PIL-Br$_x$@Zn-CTM	622	92	[108]
PIL@ZIF-8	1294	430	[109]
PIL@UiO-66-NH$_2$	977	489	[110]
Pure PIL	/	29	[110]

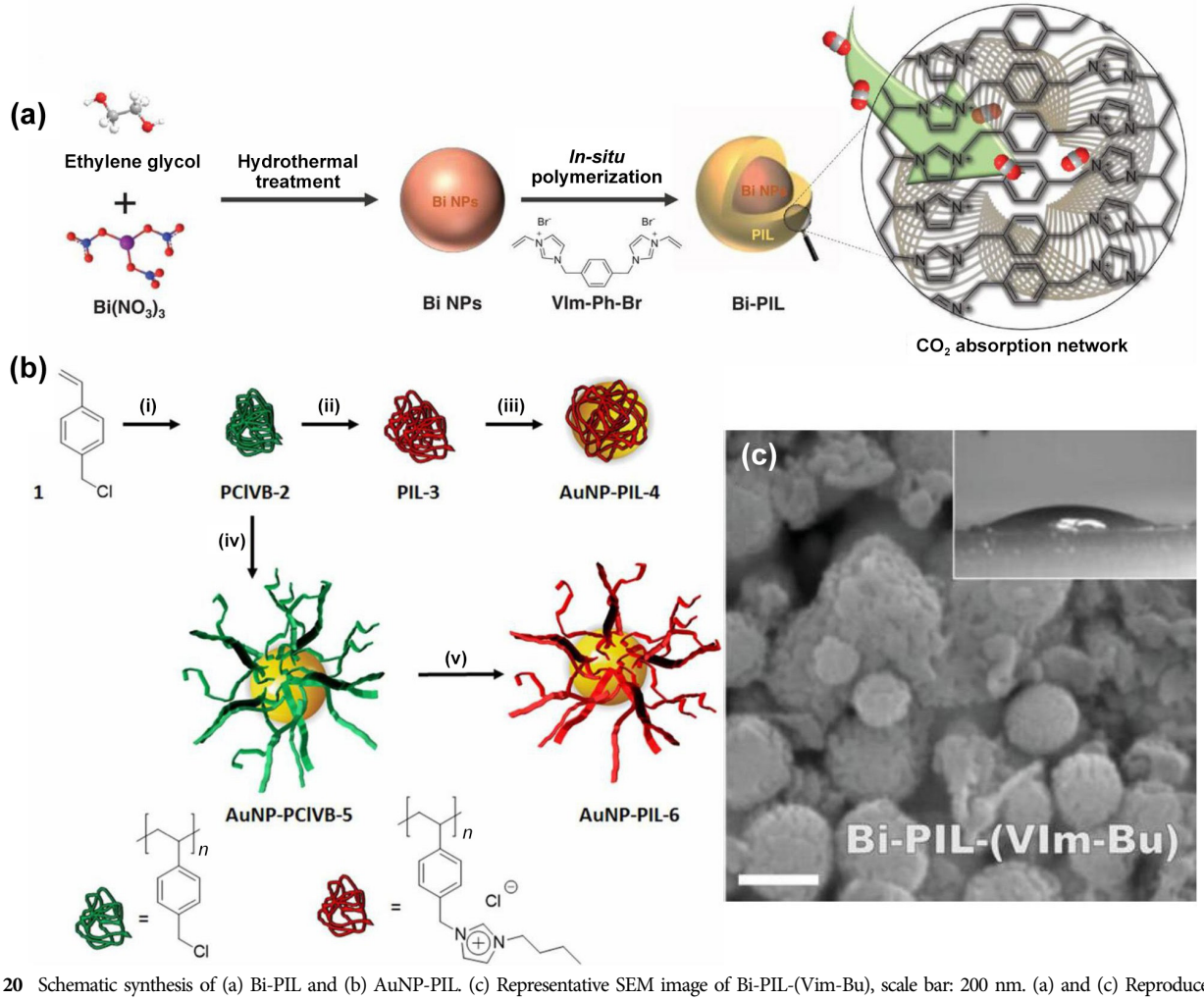

Figure 20 Schematic synthesis of (a) Bi-PIL and (b) AuNP-PIL. (c) Representative SEM image of Bi-PIL-(Vim-Bu), scale bar: 200 nm. (a) and (c) Reproduced with permission from Ref. [113], © Wiley-VCH GmbH 2024. (b) Reproduced with permission from Ref. [112], © American Chemical Society 2016.

around the Au nanoparticles. The two components independently catalyzed the Knoevenagel condensation and the reduction of substrates such as p-nitrophenol, while their combined catalytic activity enabled a one-pot, four-step consecutive reaction cascade—condensation, nitro reduction, alkene reduction, and ester reduction—in the presence of $NaBH_4$ [112].

The conductivity of metal guarantees its application electrocatalysis. A recent work by Wang's and Ye's group in 2024 achieved the direct and continuous production of pure formic acid from flue gas through molecular engineering of PIL. They designed both Bi@PIL (synthesis can be seen in Fig. 20(a), and characterization can be seen in Fig. 20(c)) and Ag@PIL hybrid catalyst by coating the Bi and Ag surface with a PIL layer via *in-situ* polymerization. The PIL layer integrates both CO_2 enrichment and synergistic catalytic functions, in which the introduction of biphenyl groups enhances hydrophobicity, while the DVB crosslinker improves structural stability. The application of a solid-state electrolyte (SSE) electrolyzer enables the integrated and continuous production of pure formic acid directly from flue gas, providing a direct, continuous, and low-carbon conversion pathway from industrial flue gas to high-value chemicals for industrial production [113].

5 Conclusion and outlook

PIL nanomaterials exhibit significant potential in fields such as catalysis and energy due to their designable molecular structures, diverse self-assembly behaviors, and unique physicochemical properties. This review systematically summarizes recent advances in their synthesis, morphological control, and catalytic applications. By selecting appropriate polymerization techniques (e.g., FRP, LRP), PILs with well-defined structures and controllable functionalities can be prepared. For specific molecular structures, PILs can self-assemble into a variety of nanostructures in selective solvents or melt states. Their final morphologies can be effectively tailored through molecular design strategies such as modifying alkyl chain length, constructing block copolymers, and exchanging counterions, as well as by employing different assembly methods like traditional post-assembly and PISA.

In catalysis, PILs can function directly as catalysts, act cooperatively with metals, or serve as stabilizers to form core–shell structures encapsulating metal centers. They are excellent supports for metal nanoparticles (e.g., Pd, Au, Cu) and metal ions. Furthermore, combining PILs with MOFs creates synergistic catalytic systems. These assemblies or composite materials show advantages in catalyzing various reactions, especially in CO_2 capture and conversion applications.

However, despite these significant achievements, the further development of this field still faces several core challenges.

(1) The precision and universality of morphology control are insufficient. The manipulation of complex topological structures remains largely empirical, lacking universal theoretical and computational models. Particularly for block copolymers, although some predictive models exist [31, 32], they primarily focus on melt states. While modified models have been proposed for solution systems, they tend to be system-specific, making experimental results the dominant factor in practical operations.

(2) The capacity for multiple catalytic cycles remains inadequate. This issue is particularly pronounced in PIL-metal composite materials, where the sintering of metal nanoparticles, leaching of metal ions, and MOF structural collapse induced by PIL incorporation are significant factors leading to catalyst deactivation. In practice, most reported systems demonstrate recyclability of no more than 10 cycles, which falls far short of the requirements for industrial applications.

(3) In chemical production, continuous flow technology offers significant advantages over traditional batch reactors in terms of heat and mass transfer, precise control of the reaction process, safety, and scalability. PIL-based catalysts, particularly those in the form of monoliths, thin films, or microchannel coatings, can be seamlessly integrated into flow systems. This integration is expected to deliver higher efficiency, extended catalyst lifetimes, and greater space-time yields for catalytic processes such as CO_2 conversion, biomass valorization, and fine chemical synthesis.

(4) In theory, stimuli-responsive catalysts are feasible based on the characteristics of PIL self-assembly: by altering the environment to adjust the morphology of PILs, thereby changing the specific surface area or exposing more active sites to regulate catalytic activity. However, the main current challenge lies in the fact that PILs with certain stimuli-responsive capabilities do not necessarily possess high loading capacity, and vice versa. How to obtain such materials through molecular design and synthesis method selection warrants further investigation.

(5) While single-atom catalysis has recently emerged as a research frontier due to its exceptional atom utilization efficiency, the precise anchoring of individual metal atoms on PIL backbones with maintained stability remains highly challenging. Furthermore, understanding the structure–activity relationship between their local coordination environment and catalytic performance presents a significant scientific hurdle.

(6) Currently, the development of artificial intelligence (AI) technology is progressing at an extremely rapid pace. Given that the molecular design of PILs is a complex and extensive endeavor, AI and machine learning (ML) technologies enable researchers to efficiently screen promising candidate materials by establishing predictive models that correlate PIL structural descriptors (e.g., monomer type, crosslinking density, counter-ion, nanoarchitecture) with catalytic performance metrics (e.g., activity, selectivity, stability).

In summary, considering the current research progress and future challenges regarding PILs, we believe future studies should focus on developing a scientific foundation for precise synthesis and unraveling the principles governing hierarchical assembly. Efforts should be directed toward creating intelligent catalytic systems with dynamic adaptability and synergistic functionalities, while actively exploring cross-disciplinary applications in emerging fields such as energy and sensing. The ultimate goal is to bridge the gap from fundamental research to practical applications. We are confident that, through persistent efforts, PIL materials will eventually replace many traditional materials, becoming cost-effective and practical alternatives.

Data availability

Not applicable.

Acknowledgements

The authors express their sincere gratitude to Zhenyu Wan from Key Lab of Organic Optoelectronics and Molecular Engineering of Ministry of Education Department of Chemistry, Tsinghua

University for her contributions to the illustration of the images in TOC. This work is granted by the National Natural Science Foundation of China (Nos. 52273106 and 52473114).

Declaration of competing interest

All the contributing authors report no conflict of interest in this work.

Author contribution statement

S. Y. Y.: Writing – original draft, and writing – review & editing, visualization, investigation. S. M. Y.: Writing – review & editing. J. Y. Y.: Supervision.

Use of AI statement

None.

References

[1] MacFarlane, D. R.; Forsyth, M.; Howlett, P. C.; Kar, M.; Passerini, S.; Pringle, J. M.; Ohno, H.; Watanabe, M.; Yan, F.; Zheng, W. J. et al. Ionic liquids and their solid-state analogues as materials for energy generation and storage. *Nat. Rev. Mater.* **2016**, *1*, 15005.

[2] Wang, X. H.; Salari, M.; Jiang, D. E.; Chapman Varela, J.; Anasori, B.; Wesolowski, D. J.; Dai, S.; Grinstaff, M. W.; Gogotsi, Y. Electrode material-ionic liquid coupling for electrochemical energy storage. *Nat. Rev. Mater.* **2020**, *5*, 787–808.

[3] Yuan, J. Y.; Mecerreyes, D.; Antonietti, M. Poly(ionic liquid)s: An update. *Prog. Polym. Sci.* **2013**, *38*, 1009–1036.

[4] Mecerreyes, D. Polymeric ionic liquids: Broadening the properties and applications of polyelectrolytes. *Prog. Polym. Sci.* **2011**, *36*, 1629–1648.

[5] Qian, W. J.; Texter, J.; Yan, F. Frontiers in poly(ionic liquid)s: Syntheses and applications. *Chem. Soc. Rev.* **2017**, *46*, 1124–1159.

[6] Zhu, M. Y.; Yang, Y. Poly(ionic liquid)s: An emerging platform for green chemistry. *Green Chem.* **2024**, *26*, 5022–5102.

[7] Wu, Y. B.; Han, L.; Zhang, X. Q.; Mao, J.; Gong, L. F.; Guo, W. L.; Gu, K.; Li, S. X. Cationic polymerization of isobutyl vinyl ether in an imidazole-based ionic liquid: Characteristics and mechanism. *Polym. Chem.* **2015**, *13*, 2560–2568.

[8] Minamimoto, H.; Irie, H.; Uematsu, T.; Tsuda, T.; Imanishi, A.; Seki, S.; Kuwabata, S. Polymerization of room-temperature ionic liquid monomers by electron beam irradiation with the aim of fabricating three-dimensional micropolymer/nanopolymer structures. *Langmuir* **2015**, *31*, 4281–4289.

[9] Li, D.; Zhang, Y. M.; Zhu, F. L.; Wang, H. P.; Wang, B. Application of ionic liquids as solvents for radical polymerization. *Chin. Polym. Bull.* **2006**, 38–46.

[10] Ohno, H.; Ito, K. Room-temperature molten salt polymers as a matrix for fast ion conduction. *Chem. Lett.* **1998**, *27*, 751–752.

[11] Hirao, M.; Ito, K.; Ohno, H. Preparation and polymerization of new organic molten salts; N-alkylimidazolium salt derivatives. *Electrochim. Acta* **2000**, *45*, 1291–1294.

[12] Zhou, Y. H.; Fei, X.; Tian, J.; Xu, L. Q.; Li, Y. A ionic liquid enhanced conductive hydrogel for strain sensing applications. *J. Colloid Interface Sci.* **2022**, *606*, 192–203.

[13] Wang, A. L.; Li, S. H.; Zhang, L. Y.; Chen, H.; Li, Y. N.; Hu, L. H.; Peng, X. Ionic liquid microemulsion-mediated *in situ* thermosynthesis of poly(ionic liquid)s and their adsorption properties for Zn(II). *Polym. Eng. Sci.* **2019**, *59*, 1036–1042.

[14] Tokuda, M.; Suzuki, T.; Minami, H. Morphological change of thermosensitive imidazolium-based poly(ionic liquid)/poly(phenylethylmethacrylate) composite particles. *Polym. Adv. Technol.* **2017**, *28*, 470–475.

[15] Lei, Q.; He, F.; Zhao, X. P.; Yin, J. B. Inorganic reinforced poly(ionic liquid) microcapsules: Confined cooling-assisted phase separation self-assembly and enhanced electroresponsive properties. *Macromol. Rapid Commun.* **2022**, *43*, 2100769.

[16] Yang, W.; He, X. J.; Gao, J. Z.; Guo, H.; He, X. Y.; Wan, F.; Zhao, X. L.; Yu, Y.; Pei, B. Synthesis, characterization, and tunable wettability of poly(ionic liquid) brushes via nitroxide-mediated radical polymerization (NMP). *Chin. Sci. Bull.* **2010**, *55*, 3562–3568.

[17] Pantazidis, C.; Andreou, S.; Glynos, E.; Sakellariou, G. Synthesis of a well-defined polyelectrolyte by controlled/"living" nitroxide-mediated radical polymerization. *Kinetic study. Eur. Polym. J.* **2020**, *134*, 109815.

[18] Cordella, D.; Kermagoret, A.; Debuigne, A.; Riva, R.; German, I.; Isik, M.; Jérôme, C.; Mecerreyes, D.; Taton, D.; Detrembleur, C. Direct route to well-defined poly(ionic liquid)s by controlled radical polymerization in water. *ACS Macro Lett.* **2014**, *3*, 1276–1280.

[19] Wu, D. H.; Wang, J. N.; Yin, X. D.; Tan, R. X.; Zhang, T. Grafting of poly(ionic liquid) brushes through Fe_0-mediated surface-initiated atom transfer radical polymerization for marine antifouling. *Langmuir* **2024**, *40*, 8393–8399.

[20] Foley, K.; Walters, K. B. Solution and film self-assembly behavior of a block copolymer composed of a poly(ionic liquid) and a stimuli-responsive weak polyelectrolyte. *ACS Omega* **2023**, *8*, 33684–33700.

[21] He, X.; Liu, G.; Zhang, Y. Z.; Li, G. X.; Niu, Y. H. Correlation between the molecular structure and multiscale dynamic relaxation in polymerized ionic liquid block copolymers. *Macromolecules* **2025**, *58*, 2276–2288.

[22] Liu, G.; Larson, R. G.; Li, L.; Luo, H.; He, X.; Niu, Y. H.; Li, G. X. Influence of chain entanglement on rheological and mechanical behaviors of polymerized ionic liquids. *Macromolecules* **2023**, *56*, 2719–2728.

[23] Wu, Y. G.; Li, T.; Li, Z. K.; Lortie, F.; Bernard, J.; Binder, W. H.; Chen, S. B.; Zhu, J. T. "Mix-and-match": Self-sorting assembly governed supramolecular polymeric nanomedicine for boosting combined chemo/phototherapy. *Adv. Mater.* **2025**, *37*, 2502416.

[24] Dong, T. T.; Xu, G. J.; Xie, B.; Liu, T.; Gong, T. Y.; Sun, C. H.; Wang, J. Z.; Zhang, S.; Zhang, X. H.; Zhang, H. R. et al. An electrode-crosstalk-suppressing smart polymer electrolyte for high safety lithium-ion batteries. *Adv. Mater.* **2024**, *36*, 2400737.

[25] Deng, Z. Y.; Qian, Y. F.; Yu, Y. Q.; Liu, G. H.; Hu, J. M.; Zhang, G. Y.; Liu, S. Y. Engineering intracellular delivery nanocarriers and nanoreactors from oxidation-responsive polymersomes via synchronized bilayer cross-linking and permeabilizing inside live cells. *J. Am. Chem. Soc.* **2016**, *138*, 10452–10466.

[26] Makhlooghiazad, F.; Mejia, L. M. G.; Rollo-Walker, G.; Kourati, D.; Galceran, M.; Chen, F. F.; Deschamps, M.; Howlett, P.; O'Dell, L. A.; Forsyth, M. Understanding polymerized ionic liquids as solid polymer electrolytes for sodium batteries. *J. Am. Chem. Soc.* **2024**, *146*, 1992–2004.

[27] Qian, S. H.; Hu, J.; You, R. M.; Wang, X. B.; Yang, L. F.; Xing, H. B.; Cui, X. L. Highly selective mixed-matrix adsorbents embedded with anion-pillared microporous materials and poly(ionic liquid)s toward sulfur dioxide capture. *Ind. Eng. Chem. Res.* **2023**, *62*, 11957–11964.

[28] Rong, L. D.; Xie, X. Y.; Yuan, W. Z.; Fu, Y. Superior, environmentally tolerant, flexible, and adhesive poly(ionic liquid) gel as a multifaceted underwater sensor. *ACS Appl. Mater. Interfaces* **2022**, *14*, 29273–29283.

[29] He, X. H.; Schmid, F. Dynamics of spontaneous vesicle formation in dilute solutions of amphiphilic diblock copolymers. *Macromolecules* **2006**, *39*, 2654–2662.

[30] Chavan, S. N.; Lee, H. I. Random ionic polymers: Salt-triggered reversible vesicular self-assembly in water. *Eur. Polym. J.* **2023**, *193*, 112114.

[31] Tang, Q. Q.; Ren, H.; Kochovski, Z.; Cheng, L. S.; Zhang, K.; Yuan, J. Y.; Zhang, W. Y. Topological effects on cyclic Co-poly(ionic liquid)s self-assembly. *Macromol. Chem. Phys.* **2023**, *224*, 2200134.
[32] Xu, H.; Niu, A. Q.; Yang, Z. W.; Wu, F. M.; Guo, X. X.; Wei, X. F.; Zhang, J. Preparation of cobalt-containing polyvinylimidazole ionic liquid catalyst and coupling with persulfate for room-temperature ultra-deep desulfurization. *Fuel* **2023**, *334*, 126762.
[33] Hu, X. F.; Li, J. Y.; Zhao, X. P.; Yin, J. B. Preparation of snowman-like poly(ionic liquid) microspheres by microwave-assisted seed emulsion polymerization. *Polymer* **2024**, *306*, 127237.
[34] May, A. W.; Shi, Z. X.; Wijayasekara, D. B.; Gin, D. L.; Bailey, T. S. Self-assembly of highly asymmetric, poly(ionic liquid)-rich diblock copolymers and the effects of simple structural modification on phase behaviour. *Polym. Chem.* **2019**, *10*, 751–765.
[35] Cordella, D.; Debuigne, A.; Jérôme, C.; Kochovski, Z.; Taton, D.; Detrembleur, C. One-pot synthesis of double poly(ionic liquid) block copolymers by cobalt-mediated radical polymerization-induced self-assembly (CMR-PISA) in water. *Macromol. Rapid Commun.* **2016**, *37*, 1181–1187.
[36] Niskanen, J.; Tousignant, M. N.; Peltekoff, A. J.; Lessard, B. H. Poly(ethylene glycol)-based poly(ionic liquid) block copolymers through 1,2,3-triazole click reactions. *ACS Appl. Polym. Mater.* **2022**, *4*, 1559–1564.
[37] Xie, X. W.; Liu, C. M.; Cao, P.; Qian, L. L.; Meng, X. L.; Dai, Z. F.; Xiong, Y. B. Poly(ionic liquid) nanogel with tunable morphologies achieved via cross-linking polymerization induced self-assembly. *Polymer* **2023**, *285*, 126371.
[38] Adeel, M.; Zhao, B. J.; Mei, H. G.; Li, L.; Zheng, S. X. Nanostructured thermosets involving epoxy and poly(ionic liquid)-Containing diblock copolymer. *Polymer* **2021**, *213*, 123293.
[39] Yang, Y. Q.; Zheng, J. W.; Man, S. K.; Sun, X. L.; An, Z. S. Synthesis of poly(ionic liquid)-based nano-objects with morphological transitions via RAFT polymerization-induced self-assembly in ethanol. *Polym. Chem.* **2018**, *9*, 824–827.
[40] Lathrop, P. M.; Sun, R.; Beyer, F. L.; Elabd, Y. A. Highly frustrated poly(ionic liquid) ABC triblock terpolymers with exceptionally high morphology factors. *Macromolecules* **2024**, *57*, 3776–3797.
[41] Tilottama, B.; Nrusingha, D.; Vijayakrishna, K. Partial anion exchange triggered helical conformation in chiral polyelectrolyte: Demonstration of "sergeants and soldiers like effect". *J. Polym. Sci.* **2025**, *63*, 1086–1094.
[42] Jiang, B.; Sun, Z. N.; Zhang, L. H.; Sun, Y. L.; Zhang, H. J.; Yang, H. W. Synthesis of a hypercrosslinked, ionic, mesoporous polymer monolith and its application in deep oxidative desulfurization. *J. Appl. Polym. Sci.* **2018**, *135*, 46280.
[43] Leibler, L. Theory of microphase separation in block copolymers. *Macromolecules* **1980**, *13*, 1602–1617.
[44] Yuan, J. Y.; Soll, S.; Drechsler, M.; Müller, A. H. E.; Antonietti, M. Self-assembly of poly(ionic liquid)s: Polymerization, mesostructure formation, and directional alignment in one step. *J. Am. Chem. Soc.* **2011**, *133*, 17556–17559.
[45] Zhang, W. Y.; Kochovski, Z.; Lu, Y.; Schmidt, B. V. K. J.; Antonietti, M.; Yuan, J. Y. Internal morphology-controllable self-assembly in poly(ionic liquid) nanoparticles. *ACS Nano* **2016**, *10*, 7731–7737.
[46] Manojkumar, K.; Mecerreyes, D.; Taton, D.; Gnanou, Y.; Vijayakrishna, K. Self-assembly of poly(ionic liquid) (PIL)-based amphiphilic homopolymers into vesicles and supramolecular structures with dyes and silver nanoparticles. *Polym. Chem.* **2017**, *8*, 3497–3503.
[47] Basak, A.; Kar, M.; Banerjee, P.; Anas, M.; Uchman, M.; Mandal, T. K. Alkyldimethylammoniumethyl methacrylate ionic liquid monomers and their poly(ionic liquid)s: Chain length dependent crystallinity, thermoresponsiveness, and self-assembly. *Chem. Asian. J.* **2025**, *20*, e202401948.
[48] Melodia, D.; Bhadra, A.; Lee, K.; Kuchel, R.; Kundu, D.; Corrigan, N.; Boyer, C. 3D printed solid polymer electrolytes with bicontinuous nanoscopic domains for ionic liquid conduction and energy storage. *Small* **2023**, *19*, 2206639.
[49] Suo, X.; Xia, L.; Yang, Q. W.; Zhang, Z. G.; Bao, Z. B.; Ren, Q. L.; Yang, Y. W.; Xing, H. B. Synthesis of anion-functionalized mesoporous poly(ionic liquid)s via a microphase separation-hypercrosslinking strategy: Highly efficient adsorbents for bioactive molecules. *J. Mater. Chem. A* **2017**, *5*, 14114–14123.
[50] Schulze, M. W.; McIntosh, L. D.; Hillmyer, M. A.; Lodge, T. P. High-modulus, high-conductivity nanostructured polymer electrolyte membranes via polymerization-induced phase separation. *Nano Lett.* **2014**, *14*, 122–126.
[51] Zhang, Q.; Fu, M. L.; Wang, C. J.; Wang, J. L.; Zhu, S. P. Preparation of poly(ionic liquid) nanoparticles through RAFT/MADIX polymerization-induced self-assembly. *Polym. Chem.* **2017**, *8*, 5469–5473.
[52] Puneet, P.; Kumar, L.; Singh, S.; Horechyy, A.; Srivastava, R. K.; Nandan, B. Reversal of handedness of ionic liquid-based chiral block copolymers via self-assembly in solution and bulk phase. *Polym. Chem.* **2022**, *13*, 1911–1919.
[53] He, H. K.; Rahimi, K.; Zhong, M. J.; Mourran, A.; Luebke, D. R.; Nulwala, H. B.; Möller, M.; Matyjaszewski, K. Cubosomes from hierarchical self-assembly of poly(ionic liquid) block copolymers. *Nat. Commun.* **2017**, *8*, 14057.
[54] Li, C. M.; Zhao, M. Z.; Gou, Z. N.; Zhao, T. D.; Han, H. M.; Zhu, K. Y.; Yuan, X. Y.; Ren, L. X. Self-assembly of core–shell magnetic bottlebrush poly(ionic liquid)s: Morphologies vs. magnetic properties. *Polym. Chem.* **2025**, *16*, 2413–2420.
[55] Demarteau, J.; de Añastro, A, F.; Shaplov, A, S.; Mecerreyes, D. Poly(diallyldimethylammonium) based poly(ionic liquid) di- and triblock copolymers by PISA as matrices for ionogel membranes. *Polym. Chem.* **2020**, *11*, 1481–1488.
[56] Depoorter, J.; Yan, X. B.; Zhang, B.; Sudre, G.; Charlot, A.; Fleury, E.; Bernard, J. All poly(ionic liquid) block copolymer nanoparticles from antagonistic isomeric macromolecular blocks via aqueous RAFT polymerization-induced self-assembly. *Polym. Chem.* **2021**, *12*, 82–91.
[57] Cordella, D.; Ouhib, F.; Aqil, A.; Defize, T.; Jérôme, C.; Serghei, A.; Drockenmuller, E.; Aissou, K.; Taton, D.; Detrembleur, C. Fluorinated poly(ionic liquid) diblock copolymers obtained by cobalt-mediated radical polymerization-induced self-assembly. *ACS Macro Lett.* **2017**, *6*, 121–126.
[58] Isik, M.; Fernandes, A. M.; Vijayakrishna, K.; Paulis, M.; Mecerreyes, D. Preparation of poly(ionic liquid) nanoparticles and their novel application as flocculants for water purification. *Polym. Chem.* **2016**, *7*, 1668–1674.
[59] Pothanagandhi, N.; Sivaramakrishna, A.; Vijayakrishna, K. Chiral anion-triggered helical poly(ionic liquids). *Polym. Chem.* **2017**, *8*, 918–925.
[60] Shah, A. H.; Li, J. Y.; Yang, H. G.; Rana, U. A.; Ranganathan, V.; Siddigi, H. M.; MacFarlane, D. R.; Forsyth, M.; Zhu, H. J. Enhancement of "dry" proton conductivity by self-assembled nanochannels in all-solid polyelectrolytes. *J. Mater. Chem. A* **2016**, *4*, 7615–7623.
[61] Scalfani, V. F.; Wiesenauer, E. F.; Ekblad, J. R.; Edwards, J. P.; Gin, D. L.; Bailey, T. S. Morphological phase behavior of poly(RTIL)-containing diblock copolymer melts. *Macromolecules* **2012**, *45*, 4262–4276.
[62] Hamley, I. W.; O'Driscoll, B. M. D.; Lotze, G.; Moulton, C.; Allgaier, J.; Frielinghaus, H. Highly asymmetric phase diagram of a poly(1,2-octylene oxide)-poly(ethylene oxide) diblock copolymer system comprising a brush-like poly(1,2-octylene oxide) block. *Macromol. Rapid Commun.* **2009**, *30*, 2141–2146.
[63] Matsen, M. W.; Bates, F. S. Conformationally asymmetric block copolymers. *J. Polym. Sci. Part B Polym. Phys.* **1997**, *35*, 945–952.
[64] Fredrickson, G. H.; Leibler, L. Theory of block copolymer solutions: Nonselective good solvents. *Macromolecules* **1989**, *22*, 1238–1250.

[65] Hamley, I. W.; Koppi, K. A.; Rosedale, J. H.; Bates, F. S.; Almdal, K.; Mortensen, K. Hexagonal mesophases between lamellae and cylinders in a diblock copolymer melt. *Macromolecules* **1993**, *26*, 5959–5970.

[66] Chen, S. X.; Li, Y. W.; Wang, Z. C.; Jin, Y.; Liu, R. X.; Li, X. G. Poly(ionic liquid)s hollow spheres nanoreactor for enhanced cyclohexane catalytic oxidation. *J. Catal.* **2022**, *411*, 135–148.

[67] Wu, Z. W.; Chen, C.; Guo, Q. R.; Li, B. X.; Que, Y. G.; Wang, L.; Wan, H.; Guan, G. F. Novel approach for preparation of poly (ionic liquid) catalyst with macroporous structure for biodiesel production. *Fuel* **2016**, *184*, 128–135.

[68] Bian, Y. H.; Zhang, J.; Zhang, S. J.; Liu, C. Z.; Zhao, D. S. Synthesis of polyionic liquid by phenolic condensation and its application in esterification. *ACS Sustain. Chem. Eng.* **2019**, *7*, 17220–17226.

[69] Gao, H. Y.; Zhou, Y. M.; Sheng, X. L.; Zhao, S.; Zhang, C.; Fang, J. S.; Wang, B. B. Alkylation of *O*-xylene and styrene catalyzed by cross-linked poly acidic ionic liquids catalyst with novel mesoporous-macroporous structure. *Appl. Catal. A Gen.* **2018**, *552*, 138–146.

[70] Shi, S. B.; Wu, W. T.; Liu, P. L.; Xiao, G. M. Sulphonic acid-functionalized polymeric ionic liquids catalyzed conversion of carbohydrates into levulinic acid in one-pot reaction. *ChemCatChem* **2023**, *15*, e202201274.

[71] Zhu, J. F.; Chen, F.; Zhang, J.; Hou, R. J.; Sun, J. K.; Zhou, X. J.; Yuan, J. Y.; Wang, X. P. Reversible switching and recycling of thermoresponsive 1,2,4-triazolium-based poly(ionic liquid) catalysts for porous organic cage synthesis in organic media. *ACS Macro Lett.* **2025**, *14*, 458–463.

[72] Chen, P. B.; Tang, X. Y.; Meng, X. J.; Tang, H. T.; Pan, Y. M.; Liang, Y. Transition metal-free catalytic formylation of carbon dioxide and amide with novel poly(ionic liquid)s. *Green Synth. Catal.* **2022**, *3*, 162–167.

[73] Ding, J.; Wang, P. R.; He, Y. T.; Cheng, L. Y.; Li, X.; Fang, C.; Li, H. P.; Wan, H.; Guan, G. F. Porous sulfonyl binuclear carbonate poly(ionic liquid)s for one-pot fixation of diluted CO_2 into dimethyl carbonate. *Appl. Catal. B Environ.* **2023**, *324*, 122278.

[74] Supasitmongkol, S.; Styring, P. High CO_2 solubility in ionic liquids and a tetraalkylammonium-based poly(ionic liquid). *Energy Environ. Sci.* **2010**, *3*, 1961–1972.

[75] Bates, E. D.; Mayton, R. D.; Ntai, I.; Davis, J. H. CO_2 capture by a task-specific ionic liquid. *J. Am. Chem. Soc.* **2002**, *124*, 926–927.

[76] Xiong, Y. B.; Wang, Y. J.; Wang, H.; Wang, R. M. A facile one-step synthesis to ionic liquid-based cross-linked polymeric nanoparticles and their application for CO_2 fixation. *Polym. Chem.* **2011**, *2*, 2306–2315.

[77] Qiu, M. Y.; Li, J.; Wu, H. N.; Huang, Y.; Guo, H. J.; Gao, D.; Shi, L. J.; Yi, Q. One-pot non-covalent heterogenization and aromatization of poly(ionic liquids) for metal-/cocatalyst-free and atmospheric CO_2 conversion. *Appl. Catal. B Environ.* **2023**, *322*, 122125.

[78] Qu, Q. H.; Cheng, L. Y.; Wang, P. R.; Fang, C.; Li, H. P.; Ding, J.; Wan, H.; Guan, G. F. Guanidine-functionalized basic binuclear poly(ionic liquid)s for low partial pressure CO_2 fixation into cyclic carbonate. *Sep. Purif. Technol.* **2024**, *339*, 126682.

[79] Jiang, Y. Q.; Yuan, X. Y.; Wang, P. R.; Cheng, L. Y.; Li, R. R.; Qu, Q. H.; Fang, C.; Li, H. P.; Ding, J.; Wan, H. et al. Dihydroxy functionalized binuclear carbonate based poly(ionic liquid)s for highly efficient conversion of low-concentration CO_2 into cyclic carbonate. *J. Environ. Chem. Eng.* **2025**, *13*, 116247.

[80] Paul, A.; Chatterjee, D.; Rajkamal; Banerjee, S.; Yadav, S. Photochemically synthesized palladium nanoparticles with catalytic activity at ppb levels for C–C coupling reactions. *RSC Adv.* **2015**, *5*, 71253–71258.

[81] Li, X.; Zhang, J.; Zhao, X. H.; Zhao, Y. Y.; Li, F.; Li, T. H.; Wang, D. J. Trace amount Pd(ppm)-catalyzed Sonogashira, Heck and Suzuki cross-coupling reactions based on synergistic interaction with an asymmetric conjugated pyridinespirofluorene. *Nanoscale* **2014**, *6*, 6473–6477.

[82] Yamada, Y. M. A.; Sarkar, S. M.; Uozumi, Y. Self-assembled poly(imidazole-palladium): Highly active, reusable catalyst at parts per million to parts per billion levels. *J. Am. Chem. Soc.* **2012**, *134*, 3190–3198.

[83] Yang, Y.; Ambrogi, M.; Kirmse, H.; Men, Y. J.; Antonietti, M.; Yuan, J. Y. Poly(ionic liquid) core turns hollow silica spheres into amphiphilic nanoreactor in water. *Chem. Mater.* **2015**, *27*, 127–132.

[84] Dani, A.; Crocellà, V.; Maddalena, L.; Barolo, C.; Bordiga, S.; Groppo, E. Spectroscopic study on the surface properties and catalytic performances of palladium nanoparticles in poly(ionic liquid)s. *J. Phys. Chem. C* **2016**, *120*, 1683–1692.

[85] Simon, N. M.; Abarca, G.; Scholten, J. D.; Domingos, J. B.; Mecerreyes, D.; Dupont, J. Structural, electronic and catalytic properties of palladium nanoparticles supported on poly(ionic liquid). *Appl. Catal. A Gen.* **2018**, *562*, 79–86.

[86] Elyasi, Z.; Ghomi, J. S.; Najafi, G. R.; Sharif, M. A. Fabrication of uniform Pd nanoparticles immobilized on crosslinked ionic chitosan support as a super-active catalyst toward regioselective synthesis of pyrazole-fused heterocycles. *Int. J. Biol. Macromol.* **2023**, *253*, 126589.

[87] Liu, Y. P.; Pan, C.; Qiu, X. M.; Zhang, H. L.; Feng, H. J.; Tang, Y. B.; Shang, Z. J.; Song, H. B. Selective oxidation of benzyl alcohol to benzaldehyde using palladium nanoparticle-loaded poly(ionic liquid)s catalysts. *Mol. Catal.* **2025**, *584*, 115273.

[88] Lau, V. M.; Pfalzgraff, W. C.; Markland, T. E.; Kanan, M. W. Electrostatic control of regioselectivity in Au(I)-catalyzed hydroarylation. *J. Am. Chem. Soc.* **2017**, *139*, 4035–4041.

[89] Jaroschik, F.; Simonneau, A.; Lemière, G.; Cariou, K.; Agenet, N.; Amouri, H.; Aubert, C.; Goddard, J. P.; Lesage, D.; Malacria, M. et al. Assessing ligand and counterion effects in the noble metal catalyzed cycloisomerization reactions of 1,6-allenynes: A combined experimental and theoretical approach. *ACS Catal.* **2016**, *6*, 5146–5160.

[90] Teller, H.; Corbet, M.; Mantilli, L.; Gopakumar, G.; Goddard, R.; Thiel, W.; Fürstner, A. One-point binding ligands for asymmetric gold catalysis: Phosphoramidites with a TADDOL-related but acyclic backbone. *J. Am. Chem. Soc.* **2012**, *134*, 15331–15342.

[91] Moghaddam, F. M.; Ayati, S. E.; Firouzi, H. R.; Hosseini, S. H.; Pourjavadi, A. Gold nanoparticles anchored onto the magnetic poly(ionic-liquid) polymer as robust and recoverable catalyst for reduction of Nitroarenes. *Appl. Organomet. Chem.* **2017**, *31*, e3825.

[92] Gai, H. J.; Zhong, C. Y.; Liu, X. F.; Qiao, L.; Zhang, X. W.; Xiao, M.; Song, H. B. Poly(ionic liquid)-supported gold and ruthenium nanoparticles toward the catalytic wet air oxidation of ammonia to nitrogen under mild conditions. *Appl. Catal. B Environ.* **2019**, *258*, 117972.

[93] Liu, Y. P.; Pan, C.; Li, X. J.; Zhang, H. L.; Shang, Z. J.; Song, H. B. Efficient conversion of HMF to FDMC utilizing gold-based poly(ionic liquid)s with bis(trifluoromethylsulfonyl)imide anion. *Chem. Eng. Sci.* **2025**, *311*, 121541.

[94] Pan, X. F.; Kochovski, Z.; Wang, Y. L.; Sarhan, R. M.; Härk, E.; Gupta, S.; Stojkovikj, S.; El-Nagar, G. A.; Mayer, M. T.; Schürmann, R. et al. Poly(ionic liquid) nanovesicles via polymerization induced self-assembly and their stabilization of Cu nanoparticles for tailored CO_2 electroreduction. *J. Colloid Interface Sci.* **2023**, *637*, 408–420.

[95] Zhang, W. Y.; Yuan, J. Y. Poly(1-vinyl-1,2,4-triazolium) poly(ionic liquid)s: Synthesis and the unique behavior in loading metal ions. *Macromol. Rapid Commun.* **2016**, *37*, 1124–1129.

[96] Liu, Y. Q.; Wang, K.; Hou, W.; Shan, W. J.; Li, J.; Zhou, Y.; Wang, J. Mesoporous poly(ionic liquid) supported palladium(II) catalyst for oxidative coupling of benzene under atmospheric oxygen. *Appl. Surf. Sci.* **2018**, *427*, 575–583.

[97] Chen, S. X.; He, B.; Li, Y. W.; Wang, R. R.; Chen, P.; Li, X. G.; Liu, R. X. Metal coordination center mediated microenvironment regulation of cobalt sites on poly(ionic liquid)s enhance selective oxidation of cyclohexane conversion. *Chem. Eng. J.* **2024**, *488*,

150865.

[98] Du, Y. R.; Li, X. Q.; Yang, X. X.; Duan, G. Y.; Chen, Y. M.; Xu, B. H. Stabilizing high-valence copper(I) sites with Cu–Ni interfaces enhances electroreduction of CO_2 to C_{2+} products. *Small* **2024**, *20*, 2402534.

[99] Beyzavi, H.; Klet, R. C.; Tussupbayev, S.; Borycz, J.; Vermeulen, N. A.; Cramer, C. J.; Stoddart, J. F.; Hupp, J. T.; Farha, O. K. A hafnium-based metal-organic framework as an efficient and multifunctional catalyst for facile CO_2 fixation and regioselective and enantioretentive epoxide activation. *J. Am. Chem. Soc.* **2014**, *136*, 15861–15864.

[100] Song, N.; Wu, Q. L.; Han, Y.; Wu, L. Y.; Zhang, D. D.; Zhang, R. R.; Fang, Y. Q.; Liu, H. D.; Chen, J.; Du, A. J. et al. The strong coordination effect on FeNi-MOF derived catalyst for durable oxygen evolution reaction over 3000 h at *operando* condition. *Nano Res.* **2025**, *18*, 94908104.

[101] Zhou, Z. F.; Wang, Y.; Lo, W. S.; Giardino, G. J.; Lalit, K.; Goldstein, M.; Wang, W. Q.; Fields, C.; Barney, A.; Tsung, C. K. et al. Processive ring-opening metathesis polymerization of low ring strain cycloalkenes via molecularly confined catalyst. *Nat. Commun.* **2025**, *16*, 8738.

[102] Fujie, K.; Kitagawa, H. Ionic liquid transported into metal-organic frameworks. *Coord. Chem. Rev.* **2016**, *307*, 382–390.

[103] Parnham, E. R.; Morris, R. E. Ionothermal synthesis of zeolites, metal-organic frameworks, and inorganic–organic hybrids. *Acc. Chem. Res.* **2007**, *40*, 1005–1013.

[104] Luo, Q. X.; Ji, M.; Lu, M. H.; Hao, C.; Qiu, J. S.; Li, Y. Q. Organic electron-rich N-heterocyclic compound as a chemical bridge: Building a Brönsted acidic ionic liquid confined in MIL-101 nanocages. *J. Mater. Chem. A* **2013**, *1*, 6530–6534.

[105] Zhou, X.; Gao, Y. J.; Deng, S. W.; Cheng, S.; Zhang, S. H.; Hu, H.; Zhuang, G. L.; Zhong, X.; Wang, J. G. Improved oxygen reduction reaction performance of co confined in ordered N-doped porous carbon derived from ZIF-67@PILs. *Ind. Eng. Chem. Res.* **2017**, *56*, 11100–11110.

[106] Ding, M. L.; Jiang, H. L. Incorporation of imidazolium-based poly(ionic liquid)s into a metal-organic framework for CO_2 capture and conversion. *ACS Catal.* **2018**, *8*, 3194–3201.

[107] Ping, R.; Zhang, H.; Wang, S. S.; Liu, F. S.; Zhang, G. J.; Wang, D. C.; Liu, M. S. Formulation of porous hetero-frameworks via incorporating poly(ionic liquid)s with porphyrin derivative-functionalized organosilicas for boosting *in-situ* CO_2 capture and conversion. *Chem. Eng. J.* **2023**, *477*, 147243.

[108] Liu, M. S.; Ma, C.; Wang, Q.; Li, R. Y.; Yu, S. Z.; Chen, H.; Liu, F. S. Capture and *in-situ* conversion of low-concentration CO_2 over robust poly(ionic liquid)@porous carbon nanocomposites under green, co-catalyst- and solvent-free conditions. *Chem. Eng. J.* **2024**, *500*, 157099.

[109] Dong, J. Q.; Zhang, H.; Ma, J. J.; Gao, K. Q.; Liu, F. S.; Li, Y. T.; Liu, M. S. Synergistic effects of core–shell poly(ionic liquids)@ZIF-8 nanocomposites for enhancing additive-free CO_2 conversion. *J. Colloid Interface Sci.* **2024**, *661*, 1000–1010.

[110] Yuan, Y. X.; Liao, Q. L.; Zhao, T. X. Synthesis of UiO-66-NH_2@PILs core–shell composites for CO_2 conversion into cyclic carbonates via synergistic catalysis under solvent- and additive-free conditions. *Colloid Surf. A Physicochem. Eng. Asp.* **2025**, *704*, 135492.

[111] Qiu, X. M.; Cao, X. Y.; Zhang, F.; Xiao, M.; Huang, T. T.; Zhu, Q. H.; Shang, Z. J.; Song, H. B. Unraveling the intermolecular interaction profiles of poly(ionic liquid)s with phenolic compounds: Insights into aromaticity, stacking, and bonding. *Fuel* **2025**, *400*, 135753.

[112] Montolio, S.; Vicent, C.; Aseyev, V.; Alfonso, I.; Burguete, M. I.; Tenhu, H.; García-Verdugo, E.; Luis, S. V. AuNP-polymeric ionic liquid composite multicatalytic nanoreactors for one-pot cascade reactions. *ACS Catal.* **2016**, *6*, 7230–7237.

[113] Li, G.; Zhang, C. Y.; Liu, Y.; Song, Y.; Guo, W. H.; Huang, L. B.; Su, J. J.; Zhang, Q.; Xin, Y. E.; Feng, T. L. et al. Molecular engineering of poly(ionic liquid) for direct and continuous production of pure formic acid from flue gas. *Adv. Mater.* **2024**, *36*, 2409390.